

**Evidence of an interaction between the actin cytoskeletal
regulators MIG-10 and ABI-1**

A Thesis

Submitted to the Faculty of

Worcester Polytechnic Institute

In partial fulfillment of the requirements for the

Degree of Master of Science

In

Biology and Biotechnology

By

Molly A McShea

Approved:

Elizabeth Ryder, PhD
Major Advisor
WPI

Luis Vidali, PhD
Committee Member
WPI

Joseph Duffy, PhD
Committee Member
WPI

Table of Contents

Figures	iv
Tables	v
Acknowledgements	vi
Abstract	viii
Introduction	1
Cell and Process Migrations Directed by <i>mig-10</i> During <i>C. elegans</i> Development	2
Molecular Mechanisms of Cell Migration and Outgrowth	6
<i>Extracellular Cues Initiate and Orient Cell Migration and Outgrowth</i>	7
<i>The MRL Family Participates in Regulation of Cytoskeletal Remodeling</i>	9
<i>MIG-10 and ABI-1 May Have Overlapping Roles in Cytoskeletal Remodeling</i>	14
Project Goals	18
Materials and Methods	20
Molecular Biology	20
Microinjection and Rescue Experiments	26
Cell Culture and Protein Expression	28
Immunoprecipitation and Western Blotting	28
Results	33
Autonomous expression of MIG-10A or MIG-10B in the excretory cell partially rescues excretory canal truncation in <i>mig-10(ct41)</i> animals	34
MIG-10A interacts with ABI-1 through either the ABI-1 N-terminus, SH3 domain, or both of these regions	37
MIG-10B interacts with ABI-1	43
Discussion	47
Further investigation is needed to determine where MIG-10 is expressed	47

MIG-10 may act both cell autonomously and cell nonautonomously during excretory canal outgrowth.....	49
The ABI-1 SH3 domain may bind multiple sites in MIG-10 to recruit Abl tyrosine kinase	54
<i>Technical considerations of co-immunoprecipitation experiments</i>	59
<i>Future experiments</i>	61
References	65

Figures

Figure 1: Phenotypes of mig-10(ct41) animals.	3
Figure 2: Excretory canal development	5
Figure 3: Lamellipodia and filopodia in an axonal growth cone	7
Figure 4: Model for MIG-10 response to guidance cue signaling	11
Figure 5: The isoforms of MIG-10	15
Figure 6: Domain structure of ABI-1	16
Figure 7: Summary of Gateway cloning strategy	21
Figure 8: Summary of nematode expression vector cloning strategy.	25
Figure 9: Overview of microinjection and transformation procedure	27
Figure 10: Overview of immunoprecipitation analysis	31
Figure 11: Cell autonomous expression of either MIG-10A or MIG-10B in the excretory cell rescued anterior canal truncation and partially rescued posterior canal truncation	35
Figure 12: Variants of MIG-10 and ABI-1 examined in the co-immunoprecipitation system	38
Figure 13: MIG-10A::V5 interacts with ABI-1::GFP but not with ABI-1(174-426)::GFP, a deletion mutant lacking the N-terminus and most of the SH3 domain	40
Figure 14: ABI-1(427-469)::GFP, a variant containing only the SH3 domain, interacts with MIG-10A::V5, MIG-10(C-term)::V5, and MIG-10(RAPH)::V5	41
Figure 15: Neither MIG-10A::V5, MIG-10(C-term)::V5, or MIG-10(RAPH)::V5 interact with ABI-1(1-173)::GFP, the variant of ABI-1 containing only the N-terminus	42
Figure 16: MIG-10B::V5 and MIG-10(RAPH)::V5 interact with ABI-1::GFP	44
Figure 17: MIG-10B::V5 and MIG-10(C-term)::V5 interact with ABI-1::GFP	45
Figure 18: Summary of results from co-immunoprecipitation analysis	55
Figure 19: Model of the physical interaction between MIG-10 and ABI-1	55
Figure 20: The interaction of ABI-1 with MIG-10 may allow for recruitment of ABL to facilitate phosphorylation of MIG-10	58
Figure 21: MIG-10 and ABI-1 are likely to function together to promote excretory canal outgrowth through a cell autonomous mechanism.	64

Tables

Table 1: Primers used for generation of AttB flanked PCR products.	22
Table 2: Primers used to generate amplicons for cloning of nematode expression vectors.	25
Table 3: DNA mixtures used for microinjection	27
Table 4: Comparison of yeast two-hybrid and co-immunoprecipitation results examining abilities of ABI-1 variants to interact with MIG-10A	57

Acknowledgements

I would like to thank my advisor, Dr. Elizabeth Ryder, for her wisdom, patience, and guidance throughout the course of my studies at WPI. Her advice and encouragement have helped me to persevere through periods of both personal and academic turbulence to become a stronger person and scientist. During my stay in her lab, her humor and optimism provided reassurance in the face of what proved to be no shortage of experimental woes.

I would like to thank the members of my committee, Dr. Luis Vidali and Dr. Joseph Duffy, for their patience, criticism, and generous offers of advice and reagents throughout the course of my project. I am particularly indebted to Dr. Duffy for allowing me the use of his lab equipment and reagents to get my co-IP experiments off the ground.

I would like to thank past and present members of the Duffy Lab for their cheerful company and support. I would especially like to thank Michelle Arata and Christina Ernst for their patient guidance through the western blotting learning process. Without them I would still be struggling to pour my first gel.

I would like to thank former and current labmates Subaiou Zhang, Mark Kuhlwein, and Sana Hashmi for their company and assistance in the lab. My experience as a graduate student certainly would have been much lonelier without them.

I would like to thank Dr. Sam Politz for his advice on rescue experiments and for allowing me to use his equipment for western blotting.

I would like to thank Dr. Claire Benard and Dr. Anne Hart for taking the time to teach me how to perform microinjections. Their expertise was invaluable to my success in generating transformants.

I would like to thank Dr. Eve Stringham and Dr. Daniel Colón-Ramos for their generous provision of reagents.

I would like to thank the Biology and Biotechnology department for teaching me and supporting me as a graduate student.

Finally I would like to give a special thanks to my parents and sister for their constant love, support, and guidance. I will always appreciate all they have done to help me get through life's tribulations and pursue my dreams.

Abstract

Cell and process migration are critical to the establishment of neural circuitry. The study of these processes is facilitated through use of model organisms with simple nervous systems, such as *C. elegans*. Research in this nematode has defined the cytoplasmic adaptor MIG-10 as a key regulator of these processes. Mutation of *mig-10* disrupts neuronal and axonal migration and outgrowth of the ‘canals’, or processes, of the excretory cell. MIG-10 directs the localization of UNC-34, which remodels actin filaments at the leading edge of a migrating cell or process to modify the direction or rate of its protrusion. An interactor of MIG-10 identified in a yeast two-hybrid analysis, ABI-1, has several roles in actin remodeling, such as targeting Ena/VASP members for phosphorylation by Abl kinase. Mutation of *abi-1* in the nematode produces phenotypes that resemble those of *mig-10* mutants, including disrupted outgrowth of the excretory canals, a developmental process in which ABI-1 is known to function cell autonomously.

To test the hypothesis that the ABI-1/MIG-10 interaction contributes to cell migration and outgrowth, both *in vivo* and *in vitro* analyses were performed. Expression of either MIG-10A or MIG-10B exclusively in the excretory cell partially rescued the canal truncation characteristic of *mig-10* mutants, suggesting MIG-10 functions autonomously in this cell during canal outgrowth. Physical interaction between MIG-10 and ABI-1 was confirmed using a co-immunoprecipitation system. Both MIG-10A and MIG-10B interact with ABI-1 through a mechanism that likely involves the SH3 domain of ABI-1 and sites in either the central region or C-terminus of MIG-10. These results suggest that MIG-10 and ABI-1 function together in a cell autonomous manner to promote cell or process migration. A possible consequence of this interaction is modulation of the MIG-10 binding to UNC-34 through Abl-mediated phosphorylation of MIG-10.

Introduction

The mature human brain is a vast network of billions of neurons that must be precisely established to enable proper function. In the cerebral cortex, the formation of this complex network begins during embryonic development in the wall of the telencephalic vesicle as progenitor cells asymmetrically divide to give rise to neurons and glia. As neurons form in the developing cerebral cortex, they organize into the six layers of mature gray matter through cell migrations guided by the processes of radial glial cells. Cortical layer formation occurs through an ‘inside-out’ mechanism by which each successive wave of migrating neurons travels from their origin in the proliferative ventricular zone outward to form a new cortical layer more peripheral to those previously formed. Once each neuron reaches its final position in the neocortex, it must then precisely extend processes to contact appropriate targets in order for a neural circuit to form (Sanes, Reh, and Harris, 2006).

Neuronal migration and axon outgrowth are vital to brain development. The impact each of these processes has on brain function can be deduced from the pathologies of diseases in which either is disrupted. For example, lissencephaly is a disease in which the layers of the neocortex fail to form correctly due to aberrant neuronal migration, and afflicted individuals suffer from severe mental retardation (Bielas *et al.*, 2004). Corpus callosum dysgenesis is a disorder that also results in mental retardation that has been attributed to defective axon guidance among neurons that normally bridge the left and right hemispheres within the corpus callosum (Engle, 2010). Careful study of the mechanisms that govern cell migration and outgrowth could not only prove useful in treating these and similar diseases, but also in developing neuroregenerative therapies and furthering our understanding of the molecular basis of complex brain function.

One of the fundamental challenges encountered by any migrating cell or extending cell process is accurate determination of the location of the destination or target. Many cells follow paths to their targets that are invariable from one organism to the next within a species, demonstrating that cells are capable of navigation that is not only accurate but also highly precise. What are the cellular and molecular mechanisms that account for this precision? Cytoskeletal remodeling provides the physical driving force behind migration and outgrowth, while the directionality of protrusion is regulated by a multitude of signal transduction pathways. While many of the molecules involved in initiation of these signaling cascades have been examined, comparatively little is known about those that lie further downstream. Therefore, this investigation focused on two cytoplasmic adaptors that link signals from the cell membrane with effectors, MIG-10 and ABI-1, in an effort to better understand their roles in regulating cytoskeletal dynamics during cell migration and outgrowth.

Cell and Process Migrations Directed by *mig-10* During *C. elegans* Development

The inherent complexity of vertebrate nervous systems renders study of their development extremely difficult. In contrast, *Caenorhabditis elegans* serves as an excellent model organism due to the simplicity of its nervous system and its genetic tractability. *C. elegans* is a microscopic, nonparasitic, soil-dwelling nematode that feeds primarily on bacteria. It can be cultured with ease in the laboratory and has a 3 day life cycle when grown optimally at 20°C. Recessive mutations can be easily maintained in the self-fertilizing hermaphrodite while the male can be used to perform crosses for genetic analysis. The adult hermaphrodite nervous system consists of 302 neurons, many of which extend processes into either the nerve ring surrounding the pharynx or bundles that run along the anterior-posterior axis of the animal. Studying the

development of these neurons and their precursors is greatly aided by the fact that *C. elegans* is transparent, allowing cells to be viewed under the microscope at all stages of the life cycle (Brenner, 1974; Wood, 1988).

The HSN, CAN, and ALM are three neurons that undergo long-range migrations in the *C. elegans* embryo (Hedgecock *et al.*, 1987). In order to identify genes necessary for these migrations, Manser and Wood conducted a screen for mutants displaying defects in CAN migration. One of the genes identified through this process was *mig-10*. In addition to disruption of the anterior-posterior migrations of the CANs, animals homozygous for *mig-10(ct41)*, which behaves as a null allele in gene dosage experiments, also display disruptions in the posteriorly-directed migrations of the ALMs and the anteriorly-directed migrations of the HSNs (Fig. 1; Manser and Wood, 1990). This null allele also has a mild effect on axon outgrowth resulting in misguidance of the axons of the HSN, AVM, and CAN (Chang *et al.*, 2006).

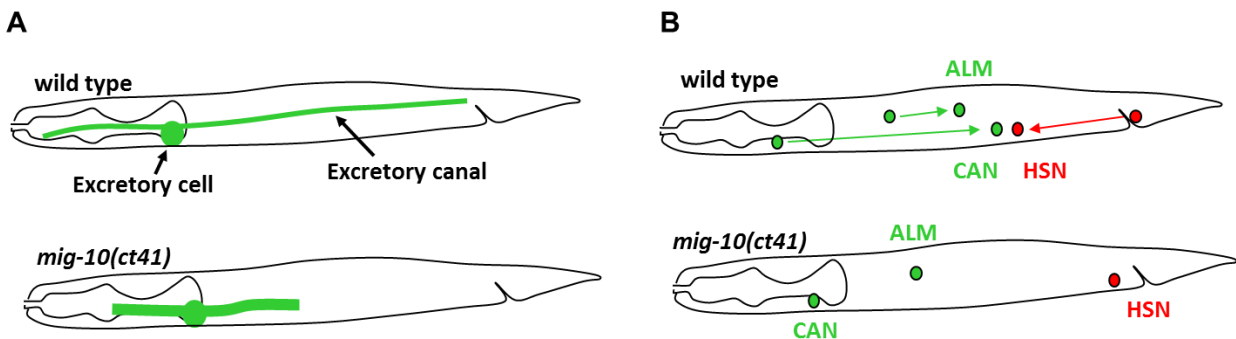


Figure 1: Phenotypes of *mig-10(ct41)* animals. (A) Both the anterior and posterior excretory canals of *mig-10(ct41)* animals are significantly shorter than in wild type animals. (B) The migrations of the ALM, CAN, and HSN are disrupted so that the positions of the cell bodies in *mig-10(ct41)* animals differ from those in wild type at the L4 stage. Arrows depict the path of migration of the associated cell, and arrowheads point to the final position of the associated cell body.

Neurons are not the only cell type affected by mutation of *mig-10*. The migration of the left coelomocyte mother cells is also disrupted in these mutants. An even more striking defect is the

severe truncation of the excretory cell processes (Manser and Wood, 1990). The excretory cell is an integral part of the *C. elegans* excretory system and functions in osmoregulation (Nelson and Riddle, 1984). The cell arises midway through embryogenesis and lies ventral to the posterior bulb of the pharynx. Soon after birth, two processes begin to emerge from the cell body and extend dorsolaterally until the tips have crossed the basement membrane secreted by the hypodermis (Fig. 2). Each process then bifurcates to extend anteriorly and posteriorly between the membranes of the hypodermal cells and the hypodermal basement membrane. Extension of these ‘canals’ continues through the L1 stage until they span nearly the entire length of the wild type animal. As the nematode continues to grow in the remaining three larval stages, a different mechanism of canal extension allows for passive lengthening to maintain the ratio of canal length to body length (Buechner, 2002). The initial phase of extension in the embryo and L1 larva is impaired in *mig-10(ct41)* animals (Hashmi and Kuhlwein, 2011), and both the posterior and anterior canals of *mig-10(ct41)* animals are significantly shorter than those of wild type when examined at the L4 stage (Fig. 1; Manser and Wood, 1990; Zhang, 2010).

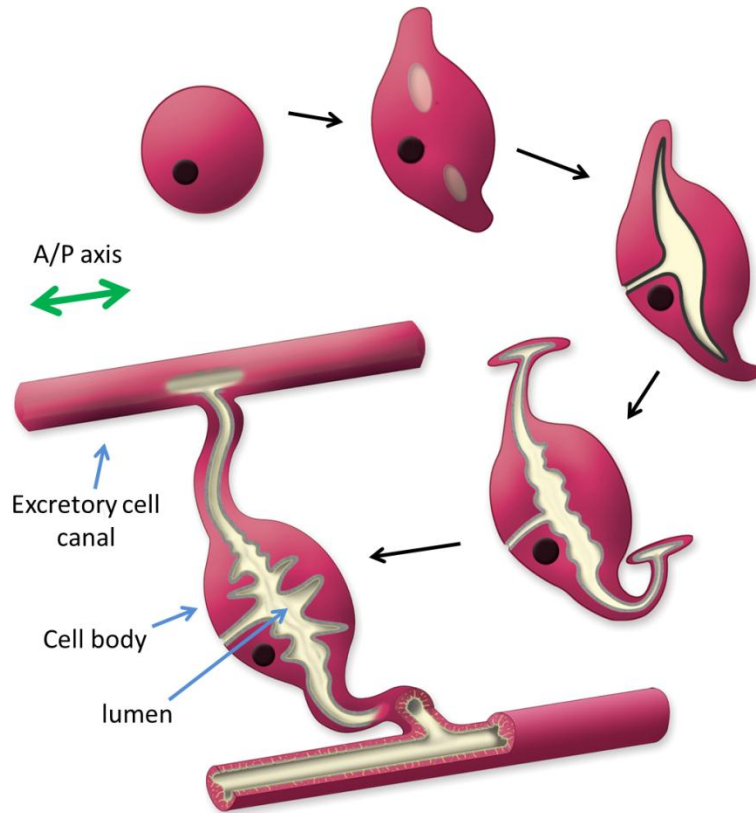


Figure 2: Excretory canal development. The excretory cell is born at the end of gastrulation. By 300 minutes past the first cell division of embryogenesis, the excretory processes begin to grow out from the cell body dorsolaterally and vacuoles begin to collect within the cell body. The vacuoles later coalesce to form the lumen, which then extends as the canals extend. Once the excretory cell processes reach the lateral hypodermis, they bifurcate and extend in both directions along the anterior-posterior axis until the end of the L1 stage. The canals continue to grow passively through the remaining larval stages as the animal grows in length (Altun and Hall, 2009).

The excretory cell defects observed in *mig-10(ct41)* mutants show that the function of *mig-10* is not exclusive to neuronal development. Moreover, many other genes necessary for neuronal and axonal migration in *C. elegans* also contribute to excretory canal outgrowth. For example, expression of *unc-6* is required to direct many axons to their proper position in the dorsal-ventral plane as well as for dorsal guidance of the excretory canals (Hedgecock *et al.*, 1987; Buechner, 2002). The biochemical mechanisms required for excretory canal outgrowth are therefore likely to be similar to those necessary for neuronal and axonal migration. However, because the

excretory cell is the largest cell in *C. elegans*, its morphology is much easier to examine than that of individual neurons (Buechner, 2002). In addition, excretory canal truncation is the only defect of the Mig-10 phenotype that is 100% penetrant (Manser and Wood, 1990). Thus, the excretory cell serves as a convenient model for studying the function of MIG-10 in cell migration and outgrowth.

Molecular Mechanisms of Cell Migration and Outgrowth

Many genes required for cell migration and outgrowth encode components of signal transduction pathways. Signal transduction contributes to the regulation of many cellular processes and generally consists of a complex chain of molecular interactions and events that functions to transduce a cue from the environment into specific changes within the cell. In the case of cell migration and outgrowth, the outcome of many pathways regulating these processes is modification of the actin cytoskeleton at the leading edge of the cell. In particular, the polymerization of actin filaments is necessary for the formation of protrusions such as lamellipodia and filopodia (Fig. 3), which contribute to translocation of the leading edge—and the cell or process—toward the target. Much evidence now suggests that MIG-10 and its vertebrate homolog Lamellipodin serve a critical role in relaying signals from the cell surface to effectors that directly modify F-actin and allow for tight regulation of the orientation of protrusions from the leading edge (Quinn and Wadsworth, 2008).

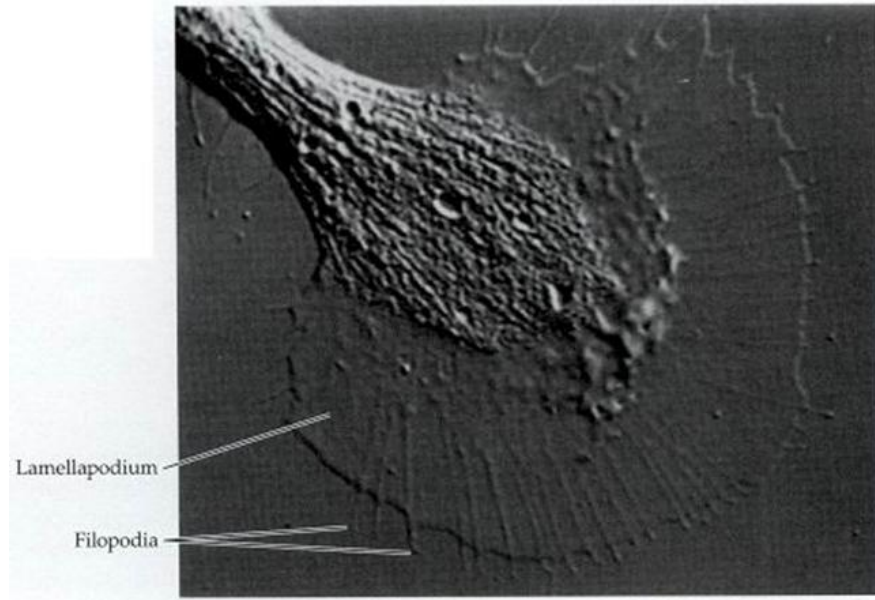


Figure 3: Lamellipodia and filopodia in an axonal growth cone. Lamellipodia are composed of dense meshworks of actin filaments while filopodia are long, finger-like projections from the leading edge containing highly bundled actin filaments (Purves, *et al.*, 2001).

Extracellular Cues Initiate and Orient Cell Migration and Outgrowth

Of the wide variety of molecules that activate cytoskeletal pathways contributing to cell migration and outgrowth, perhaps some of the best studied are the four classical families of guidance cues. These cues and their pathways are highly conserved and consist of the netrins, slits, semaphorins, and ephrins. The first three families consist of secreted molecules that can function as both short-range and long-range cues while the ephrins are membrane-bound molecules that can only direct the migrations of nearby axons or cells. A common characteristic of all these families is that members of each can often elicit either chemoattraction or chemorepulsion of a migrating cell or process, and the distinction between these two modes is usually determined by the receptor expression profile of the migrating cell or process (Kolodkin and Tessier-Lavigne, 2010). For example, the *C. elegans* netrin family member UNC-6 attracts

cells expressing the UNC-40 receptor and repels cells expressing the UNC-5 receptor alone or in combination with UNC-40 (Hedgecock, Culotti, and Hall, 1990; Chan *et al.*, 1996).

Aside from classical guidance cues, morphogens and cell adhesion molecules have also been shown to direct cell migration and outgrowth in *C. elegans*. Some of these molecules act as guidance cues while others stimulate cell migration and outgrowth through slightly different mechanisms. The Wnt family member EGL-20 is an interesting example of a molecule that does both. EGL-20 acts as a chemorepellent in directing the migrations of the HSNs and growth cones of the AVM and PVM axons anteriorly (Pan *et al.*, 2006), but it also stimulates neurons of the QL lineage to migrate posteriorly by another mechanism involving dose-dependent activation of the Hox gene *mab-5* (Whangbo and Kenyon, 1999). Many other members of these families of signaling molecules do not directly stimulate cell migration or outgrowth at all, but rather modify the cell's sensitivity or response to certain guidance cues. For example, the BMP-like protein UNC-129 influences the sensitivity of dorsally migrating cells and growth cones to UNC-6 by increasing UNC-5/UNC-40 co-expression as migration proceeds down the UNC-6 gradient (MacNeil *et al.*, 2009). Autonomous expression of the integrin INA-1 by migrating cells of the Q lineage is necessary for their proper migration and changes in the levels of expression may change the rate at which these cells migrate (Ou and Vale, 2009).

The SLT-1/Slit receptor SAX-3/Robo mediates repulsion of cells on which it is expressed from sources of SLT-1, while, as previously described, UNC-6/Netrin serves as either an attractive or repulsive cue depending on the receptors present on the surface of the migrating cell or process (Hao *et al.*, 2001; Hedgecock, Culotti, and Hall, 1990; Chan *et al.*, 1996). Opposing gradients of SLT-1 and UNC-6 exist along the dorsal-ventral axis in *C. elegans*, and these cues have long been thought to function solely in positioning migrating cells or processes within this plane

(Hedgecock, Culotti, and Hall, 1990; Wadsworth, Bhatt, and Hedgecock, 1996). However, the posterior migration of the CANs is also dependent on SLT-1 (Hao *et al.*, 2001). More recent studies have shown that increased activity of either SAX-3 or UNC-40 can redirect migrating growth cones along the anterior-posterior axis, implicating UNC-6 and SLT-1 signaling in positioning migrating cells and growth cones within this plane (Levy-Strumpf and Culotti, 2007; Watari-Goshima *et al.*, 2007). MIG-10 functions downstream of both UNC-6 and SLT-1 (Quinn *et al.*, 2006) suggesting the emerging roles for these cues in anterior-posterior guidance may explain why mutation of *mig-10* disrupts migrations of cells that occur along this axis.

Some of the cells that migrate along this axis in a MIG-10-dependent fashion are regulated by signaling molecules other than UNC-6 and SLT-1. For example, the anterior migrations of the HSNs are disrupted in various Wnt mutants (Pan *et al.*, 2006) but are unaffected by mutation of *unc-6*. These observations suggest that at least in this cell, MIG-10 may function downstream of signaling molecules other than UNC-6 or SLT-1.

The MRL Family Participates in Regulation of Cytoskeletal Remodeling

How do signals at the cell surface influence the activity of MIG-10 to bring about changes in the actin cytoskeleton? A key to uncovering the connection between guidance cue detection and MIG-10-mediated responses came from observations of MIG-10 overexpression in the AVM and PVM neurons. These neurons normally are each monopolar, extending a single axon ventrally under the direction of UNC-6 and SLT-1. However, when these cells overexpressed MIG-10 in the absence of UNC-6 and SLT-1, many neurons developed a multipolar phenotype with axons that were misguided. When MIG-10 was overexpressed in the presence of either UNC-6 or SLT-1, the multipolar phenotype was suppressed and guidance was enhanced in comparison to neurons that did not overexpress MIG-10 (Quinn *et al.*, 2006). Considering that Lamellipodin

(Lpd), one of the vertebrate homologs of MIG-10, localizes to lamellipodia and filopodia in cultured cells (Krause *et al.*, 2004), one explanation for these results is that MIG-10 promotes outgrowth and that its localization is normally directed by guidance cues to control the orientation of the protrusion. Subsequent experiments examining axon outgrowth in the HSN demonstrated that MIG-10 localizes in response to UNC-6 signaling through UNC-40 to the edge of the cell closest to the UNC-6 source, and that this localization is necessary for the establishment of asymmetry that precedes axon outgrowth (Adler, Fetter, and Bargmann, 2006).

Molecular characterization of MIG-10 and one of the vertebrate members of the MRL family of proteins, Lamellipodin, revealed the physical basis for membrane localization of these proteins in response to guidance cues (Fig. 4). Both proteins contain highly conserved Ras association (RA) and pleckstrin homology (PH) domains (Krause *et al.*, 2004). A fragment of MIG-10 consisting of only these two domains was sufficient for binding specifically to the GTP-loaded human Rho GTPase Rac in a GST pulldown assay. Binding to Rac-GTP was also observed for full length MIG-10 and Lamellipodin. Mutation of *ced-10*, the gene encoding a *C. elegans* ortholog of Rac, resulted in a loss of enrichment of MIG-10 at the ventral periphery of the HSN seen in wild type animals during the L3 stage (Quinn, Pfeil, and Wadsworth, 2008). An independent set of experiments focusing on Lamellipodin demonstrated that its PH domain binds specifically to PI(3,4)P₂ in a protein lipid overlay assay (Krause *et al.*, 2004). Mutation of the gene encoding the kinase AGE-1, the *C. elegans* ortholog of PI3K, or mutation of the gene encoding DAF-18, the *C. elegans* ortholog of the phosphatase PTEN, disrupted the ventral enrichment of MIG-10 in the HSN (Adler, Fetter, and Bargmann, 2006). Both *ced-10; mig-10* and *age-1; mig-10* double mutants were analyzed with respect to axonal misguidance of the AVM, and the phenotype for each was found to be no more severe than that of *mig-10* single mutants, suggesting *mig-10*

functions in the same pathway as *ced-10* and *age-1* (Chang *et al.*, 2006). Moreover, epistasis testing placed *mig-10* downstream of both *ced-10* and *age-1* (Chang *et al.*, 2006; Quinn, Pfeil, and Wadsworth, 2008). Taken together, these results support a model in which the activation of CED-10 and AGE-1 in response to guidance cue stimulation leads to localized recruitment of MIG-10 to specific regions of the cell membrane.

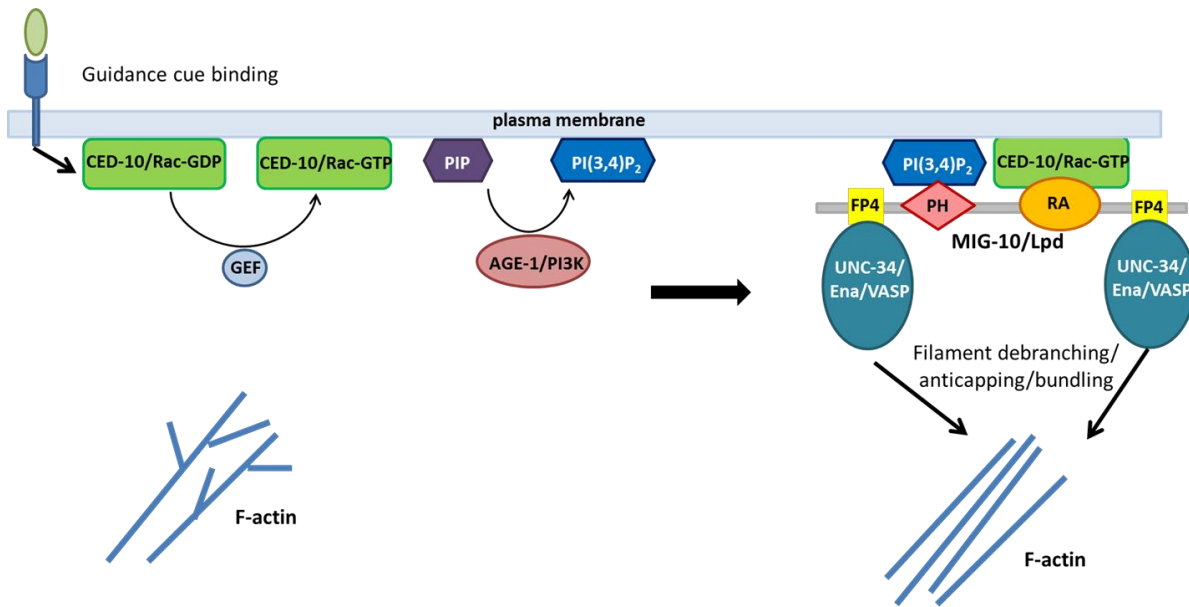


Figure 4: Model for MIG-10 response to guidance cue signaling. Guidance cue signaling stimulates activation of Rac and AGE-1, which phosphorylates phosphatidylinositol phosphate in the plasma membrane to form phosphatidylinositol (3,4) biphosphate. These molecules then recruit MIG-10 to the plasma membrane through its pleckstrin homology (PH) and Ras-association (RA) domain. UNC-34 is recruited to the same regions through binding of its EVH1 domain to FPPPP motifs in MIG-10. UNC-34 can then participate in cytoskeletal remodeling by promoting actin filament debranching, anticapping, or bundling activities.

The observed outgrowth-promoting activities of MIG-10 and Lamellipodin can be explained by the presence of a third conserved domain, the proline-rich EVH1 binding site. EVH1 binding sites are defined by the FPPPP motif with the consensus sequence

(D/E)(F/L/W/Y)PPPPX(D/E)(D/E) and bind to the EVH1 domain of proteins of the Ena/VASP family (Krause *et al.*, 2004). The six EVH1 binding sites in Lamellipodin bind directly to the

Ena/VASP family member VASP while fragments of MIG-10 containing each of two putative EVH1 binding sites have been shown to bind directly to UNC-34, the only Ena/VASP family member in *C. elegans* (Krause *et al.*, 2004; Chang *et al.*, 2006; Quinn *et al.*, 2006). Another Ena/VASP family member, Mena, co-immunoprecipitated with Lamellipodin from the lysates of cortical neurons, suggesting these proteins interact *in vivo*. Members of the Ena/VASP family colocalize with Lamellipodin to the tips of lamellipodia and filopodia in fibroblasts through a mechanism that involves both the EVH1 domain and F-actin binding EVH2 domain (Krause *et al.*, 2004). Ena/VASP members bind to the barbed ends of actin filaments and function both to bundle these filaments together and to enhance filament elongation by protecting the barbed ends from capping protein, which binds to barbed ends to prevent the addition of G-actin. Ena/VASP proteins also decrease filament branching by a mechanism that is poorly understood (Drees and Gertler, 2008). The overall effect of these activities is to promote filopodia formation. Accordingly, the filopodia that are normally present in the leading edge of HSNs during the L2 and L3 stages were almost completely lost in *unc-34* mutants, whereas overexpression of UNC-34 caused the HSNs to display about three times as many filopodia as are found in cells from wild-type animals. Mutation of *mig-10* strongly suppressed the excessive filopodia phenotype of cells overexpressing UNC-34, suggesting that MIG-10 coordinates UNC-34 during filopodia formation (Chang *et al.*, 2006). Consistent with this, expression of an EVH1 binding site coupled to a mitochondrial anchor disrupted the localization of Ena/VASP proteins in fibroblasts and suppressed the enhanced lamellipodial protrusion velocity caused by overexpression of Lamellipodin (Krause *et al.*, 2004). Displacement of Ena/VASP proteins from the cell periphery did not affect Lamellipodin's localization (Krause *et al.*, 2004). Thus, MIG-10/Lamellipodin recruits Ena/VASP proteins to the leading edge to promote protrusion (Fig. 4).

Although Ena/VASP proteins are now well established as components of the MIG-10/Lamellipodin pathway, there is evidence of additional roles for MIG-10/Lamellipodin in the regulation of cell migration and outgrowth. For example, single mutants of *mig-10* and *unc-34* have mild defects in guidance of the AVM axon while *unc-34* mutants in which the dosage of *mig-10* is reduced show a higher prevalence of AVM guidance defects compared to either single mutant (Quinn *et al.*, 2006). *mig-10; unc-34* double mutants die between midembryogenesis and the third larval stage, and those that survive into the L2 stage display severe defects in AVM axon guidance (Chang *et al.*, 2006). The enhancement in the severity of AVM guidance defects observed in double mutants relative to the single mutants suggests that MIG-10 and UNC-34 are likely to each have other functions in regulating cell migration and outgrowth that are non-overlapping.

Analysis of other MRL family members has uncovered roles for these proteins outside of the regulation of cell migration and outgrowth. RIAM is another vertebrate homolog of MIG-10 that contains the RA, PH, and EVH1 binding sites that define all members of the MRL family. Unlike Lamellipodin and MIG-10, RIAM binds to the GTPase Rap1 and assists in its localization to the cell membrane, where it promotes integrin-mediated adhesion (Lafuente *et al.*, 2004). The *Drosophila* MRL family member Pico appears to promote cell proliferation and tissue growth in response to changes in G:F actin ratios through an EGFR-dependent mechanism. This mechanism is conserved in mammalian cells in which Lamellipodin acts homologously to Pico, demonstrating a previously unrecognized function for Lpd outside cell migration and outgrowth (Lylulcheva *et al.*, 2008). It is therefore likely that the full extent to which MIG-10 and other MRL members contribute to regulation of the actin cytoskeleton has yet to be realized.

MIG-10 and ABI-1 May Have Overlapping Roles in Cytoskeletal Remodeling

The *mig-10* gene encodes a total of three potential alternatively spliced transcripts that differ only in their 5' ends (Fig. 5). The three potential isoforms of MIG-10, termed MIG-10A, MIG-10B, and MIG-10C, each contain the RA, PH, and N- and C-terminal EVH1 binding sites, but differ in the length and sequence of their N-termini. The ct41 null allele of *mig-10* contains a stop codon in exon three that prematurely truncates all three isoforms, preventing expression of the region that contains the RA and PH domains (Manser, Roonprapunt, and Margolis, 1997). Emerging evidence suggests that MIG-10A and MIG-10B may have distinct developmental roles, and that MIG-10A may be the isoform most relevant to neuronal migration and outgrowth (D. Colón-Ramos, personal communication).

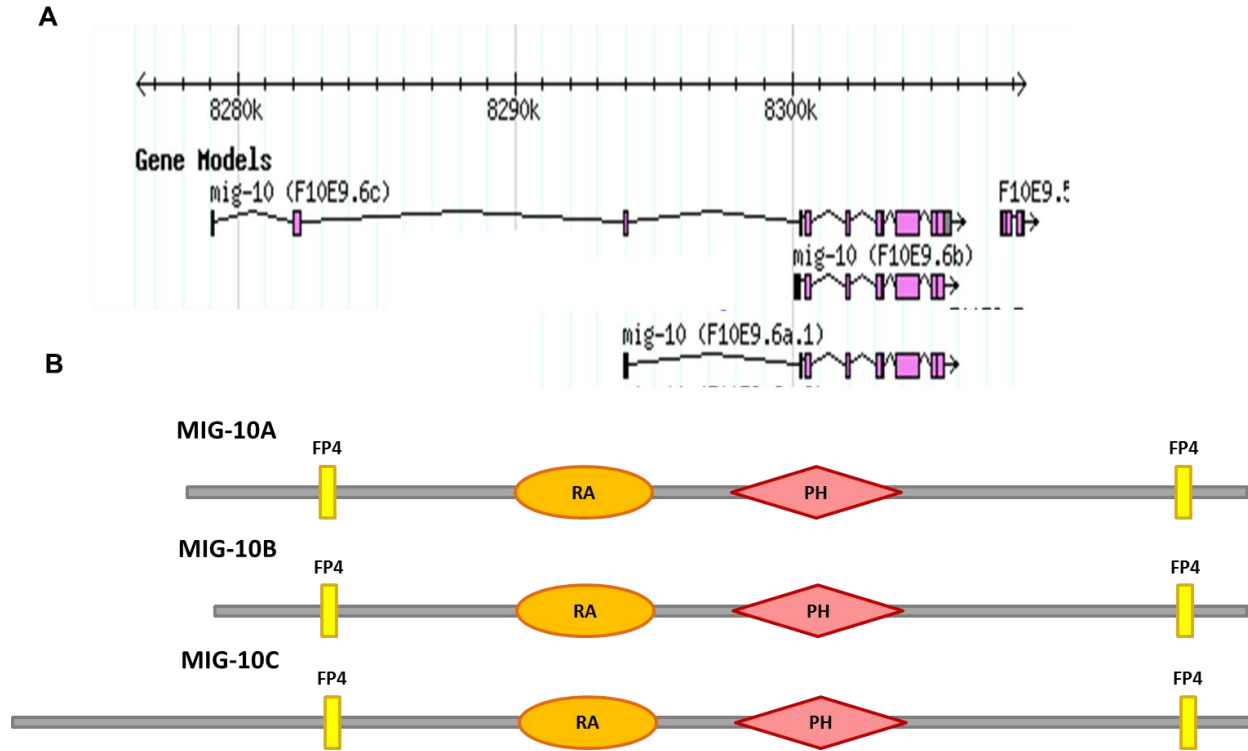


Figure 5: The isoforms of MIG-10. (A) The *mig-10* gene encodes three alternative transcripts that differ in the 5' ends. (B) The RA and PH domains and both putative EVH1 binding sites (yellow boxes) are conserved in all three isoforms. MIG-10C, the longest isoform, contains over 100 additional residues in the N-terminus compared to the smallest isoform, MIG-10B. Regions of proline-rich sequence exist in several locations along the length of each isoform and are most concentrated in the region between the PH domain and the C-terminal EVH1 binding site (modified from WormBase, <http://www.wormbase.org>).

Efforts to elucidate additional mechanisms of MIG-10-mediated regulation of cell migration and outgrowth turned to identification of protein interactors of MIG-10A. A yeast two-hybrid analysis using MIG-10A as bait was employed to screen the entire *C. elegans* cDNA library for interactors. Of the proteins identified as potential interactors, ABI-1 was the strongest candidate after having been isolated upon each of six independent transformations of the entire cDNA library (Gosselin and O'Toole, 2008). Consistent with this result, animals homozygous for *abi-1(tm494)*, a hypomorphic allele of *abi-1*, displayed truncated excretory canals, defects in ALM cell migration, and misguidance of the AVM axon. These defects resemble those observed in

mig-10(ct41) mutants, suggesting that ABI-1 and MIG-10 function in similar developmental processes in *C. elegans* (Schmidt *et al.*, 2009; Dubuke and Grant, 2009; Sullivan-Keizer, 2009).

Abelson-interactor-1 (Abi-1) was first identified as a physical interactor and downstream target of Abelson (Abl) tyrosine kinase (Shi, Ålin, and Goff, 1995). Abi family members are highly conserved. *D. discoideum*, *D. melanogaster*, and *C. elegans* each possess a single Abi family member while humans and mice have three Abi family members. As shown in Fig. 6, the N-terminus of ABI-1 contains an ABL-interactor homeodomain homologous region (ABL-HHR) and a SNARE domain, while the C-terminus contains a Src-homology-3 (SH3) domain (Shi, Ålin, and Goff, 1995; Echarri *et al.*, 2004). The SNARE domain of mammalian Abi-1 mediates binding to Syntaxin-1, implicating a role for Abi-1 in the regulation of vesicle fusion with the cell membrane (Echarri *et al.*, 2004). SH3 domains bind proline-rich sequences to mediate protein-protein interactions and in the case of mammalian Abi-1, this domain has been implicated in binding to Abl kinases and the ubiquitin ligase Cbl (Shi, Ålin, and Goff, 1995; Tanos and Pendergast, 2007).

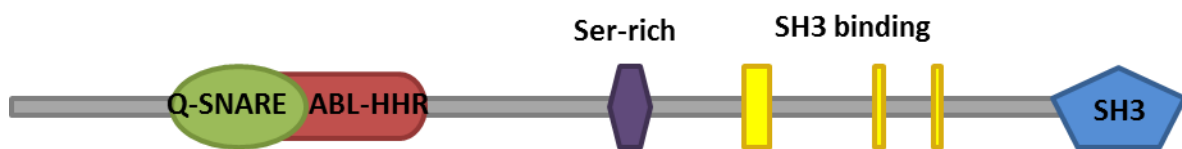


Figure 6: Domain structure of ABI-1. Overlapping Q-SNARE and ABL-HHR domains are found in the N-terminus. The central region of the protein contains a serine-rich region and SH3 binding sites. The C-terminus contains an SH3 domain (Schmidt *et al.*, 2009).

The best-characterized role for ABI-1 in cytoskeletal regulation is its participation in the WAVE regulatory complex (WRC). WASP and WAVE proteins are found in all metazoans and are the targets of many signal transduction pathways. They become activated and localized by

phosphorylation, GTPase binding, and phosphoinositide binding, all of which occur in response to upstream signaling events (Takenawa and Suetsugu, 2007; Leng *et al.*, 2005; Oikawa *et al.*, 2004). Once activated, these proteins stimulate the Arp2/3 complex to nucleate and branch actin filaments (Goley and Welch, 2006). In cultured fibroblasts, the formation of lamellipodia in response to Rac signaling is dependent on WAVE (Takenawa and Suetsugu, 2007).

Whereas WASP proteins bind directly to the GTPase Cdc42 to become activated, WAVE proteins do not bind directly to GTPases. Instead, GEX-2/Sra-1, a member of the WAVE regulatory complex, mediates binding to Rac GTPase to allow for WAVE activation (Takenawa and Suetsugu, 2007; Chen *et al.*, 2010). The WRC is pentameric and, in addition to WAVE-1/WAVE, ABI-1, and GEX-2/Sra-1, also includes the proteins GEX-3/Nap-1 and HSPC300 (Eden *et al.*, 2002; Stovold, Millard, and Machesky, 2005). Initial studies into the effects of the complex on WAVE activity yielded conflicting results, leading to the alternative hypotheses that either complex disassembly is necessary for WAVE activation or that localization of an inherently active complex is the principle means of regulation of its activity (Eden *et al.*, 2002; Innocenti *et al.*, 2004). These views were challenged by studies that showed that WRC integrity is essential for WAVE stability, the WRC remains intact regardless of whether it is in the presence or absence of active Rac, and that Rac stimulation is necessary for the WRC to activate the Arp2/3 complex (Steffan *et al.*, 2004; Rogers *et al.*, 2003; Blagg *et al.*, 2003; Ismail *et al.*, 2009). In support of these observations, examination of the structure of the crystallized WRC suggests that a conformational change in the complex upon Rac binding or phosphorylation exposes the catalytic VCA region of WAVE involved in Arp2/3 activation without leading to complex disassembly (Chen *et al.*, 2010). In mammals, Abi-1 promotes WAVE activation by

mediating its phosphorylation by Abl and may also be necessary for WRC localization to the cell membrane (Leng *et al.*, 2005).

ABI-1 has many other roles in the regulation of cytoskeletal dynamics independent of its participation in the WRC. In cultured mammalian cells, complexes containing Abi-1 and Diaphanous related formins, which nucleate unbranched actin filaments, were found to be critical for the formation of cell-cell junctions (Ryu *et al.*, 2009). Recent work in *C. elegans* demonstrated that ABI-1 interacts with the scaffolding protein UNC-53/NAV2 and that this interaction may be necessary for outgrowth of the excretory cell canals along the anterior-posterior axis (Schmidt *et al.*, 2009). Abi-1 forms a complex with Eps8 and the GEF Sos-1 in mammalian cells that responds to Ras activation through interactions with PI3K to elicit the Rac-GEF activity of Sos-1, leading to Rac activation (Scita *et al.*, 1999; Innocenti *et al.*, 2003). Analysis of the mammalian Ena/VASP family member Mena revealed that it interacts with Abi-1 in mammalian cells and that this interaction allows for regulation of phosphorylation of Mena by Abl (Tani *et al.*, 2003). Interestingly, genetic evidence from *D. melanogaster* and *C. elegans* suggests that Ena/UNC-34 and ABI-1 function together in cytoskeletal remodeling and antagonize Abl tyrosine kinase (Bashaw, *et al.*, 2000; Sheffield *et al.*, 2007; Lin *et al.*, 2009). Lamellipodin has also been identified as a substrate of Abl, but this modification appears to positively regulate Ena/VASP activity by enhancing binding to Lpd (Michael *et al.*, 2010). Presently, no role for Abi-1 in the interaction between Abl and Lpd has been reported.

Project Goals

The goal of this work was to further characterize the MIG-10/ABI-1 interaction observed in the yeast two-hybrid system. A recent study focusing on ABI-1 suggests that this protein functions cell autonomously in the excretory cell to promote canal outgrowth (Schmidt *et al.*, 2009).

However, mosaic analysis suggests that *mig-10* is required cell nonautonomously for excretory canal development, which conflicts with a model in which MIG-10 and ABI-1 function together to drive excretory canal outgrowth (Manser, Roonprapunt, and Margolis, 1997). To address this discrepancy, expression of cDNAs encoding MIG-10A and/or MIG-10B was restricted to the excretory cell in a *mig-10(ct41)* background to determine if either isoform can function cell autonomously. Secondly, an insect cell expression system was employed to examine the physical basis for the MIG-10/ABI-1 interaction through co-immunoprecipitation and western blotting.

Materials and Methods

Molecular Biology

Constructs intended for use in the immunoprecipitation system were created using the Invitrogen Gateway cloning system (Fig. 7). The primers shown in Table 1 were designed to generate amplicons encoding the desired deletion mutants of MIG-10 and ABI-1 in which the 5' and 3' ends of each coding sequence were flanked by modified attB1 and B2 Gateway recombination sites, respectively. PCR products were then generated using 0.5 units of Vent polymerase (NEB), 20 pmol of each primer, and 4 ng of the appropriate template. The template for these reactions was either a construct containing the coding sequence for mig-10a in the pDEST32 backbone or a construct containing the coding sequence for abi-1 in the pPC86 backbone, both of which were previously used in the yeast two-hybrid system (Gosselin and O'Toole, 2008). To confirm the presence of a product of the expected size, 10% of the total volume of each PCR reaction was analyzed on a 0.8% agarose gel in TAE buffer. BP reactions were then performed for each PCR product by mixing 150 ng each of pDONR vector and PCR product with 2 μ L of BP Clonase II enzyme mix (Invitrogen) and incubating these mixtures for 1 hr. at 25°C. 3 μ L of each reaction was then transformed into 50 μ L of Max-Efficiency DH5 α *E. coli* chemically competent cells (Invitrogen) and plated on LB-agar supplemented with 50 μ g/ μ L kanamycin. Plates were incubated overnight at 37°C and colonies selected the following day were individually picked to 5 mL aliquots of liquid LB medium supplemented with 50 μ g/ μ L kanamycin. Liquid cultures were grown overnight at 37°C. Plasmid DNA was isolated from these cultures using the QIAprep Spin Miniprep kit (Qiagen). Candidate entry clones were screened by restriction digest and the identities of positively selected candidates were confirmed by sequence analysis performed at the DNA Analysis Facility at Yale University.

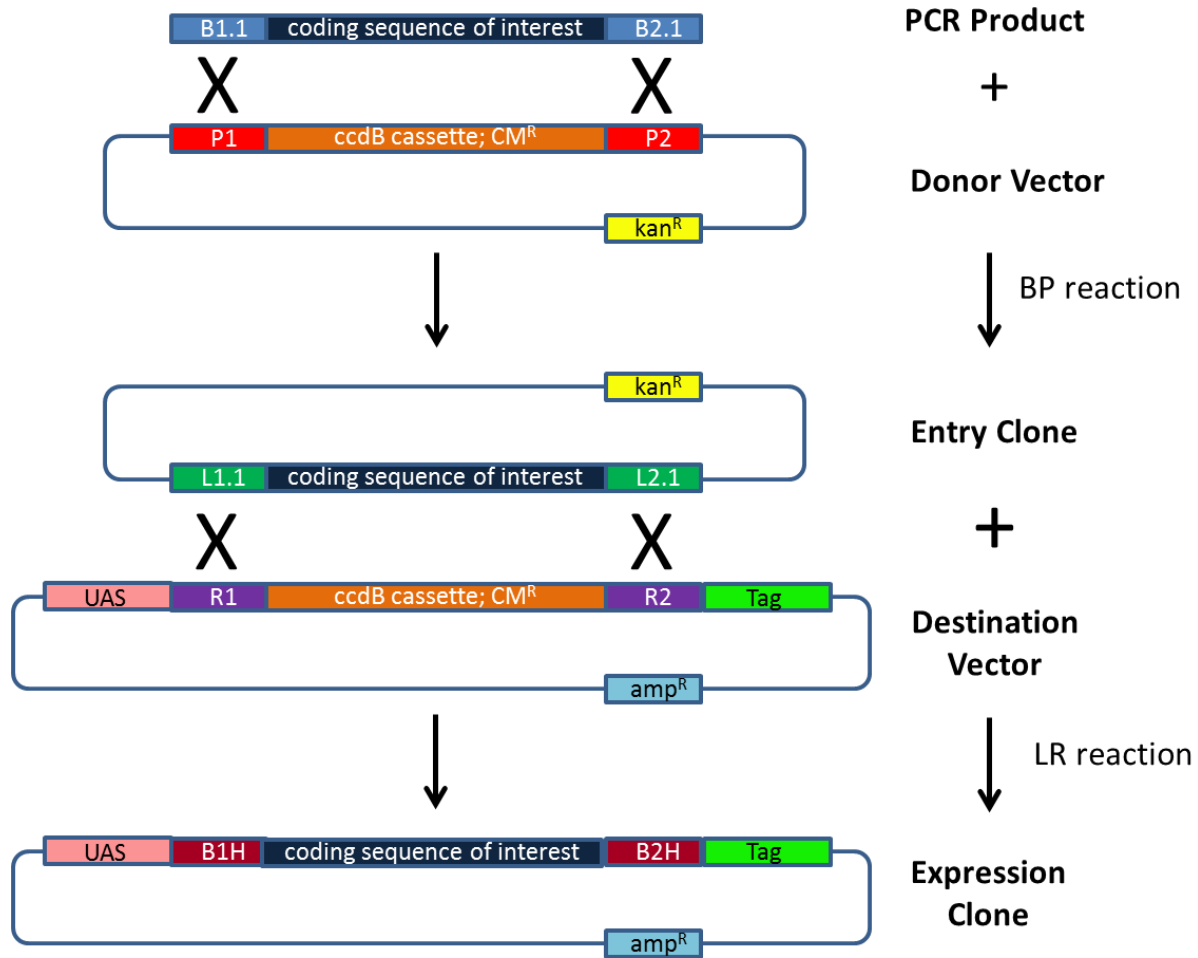


Figure 7: Summary of Gateway cloning strategy. Each PCR product encoding a variant of MIG-10 and ABI-1 of interest were generated with attB1.1 and attB2.1 sites (slightly modified from Invitrogen attB1 and attB2 sites). Recombination between these sites and attP sites in the donor vector during the BP reaction generated an entry clone containing the sequence encoding the variant of interest flanked by attL sites. Cells transformed with any unreacted donor vector were negatively selected by the ccdB cassette. Recombination between these attL sites and attR sites in a destination vector containing a UAS element and either a GFP or V5/6XHis tag moved the coding sequence of the variant of interest into the destination vector. Each expression clone produced from the LR reaction contained the sequence encoding the variant of interest flanked by att sites that were hybrids of the original and modified attB sites (referred to as B1H and B2H).

Table 1: Primers used for generation of AttB flanked PCR products. Primer names and sequences used to produce the indicated amplicons are shown.

¹ Primers designed by M. Dubuke and T. Grant as previously described (Dubuke and Grant, 2009).

Primer Name	Forward or Reverse	Deletion Mutant(s) Encoded by Generated Amplicon(s)	Sequence
abiForatt ¹	Forward	ABI-1(1-173)	5' GGG GAC AAC TTT GTA CAA AAA AGT TGG AAA ATG AGT GTT AAT GAT CTT CAA GAG 3'
abi-1_A1_R	Reverse	ABI-1(1-173)	5' GGG GAC AAC TTT GTA CAA GAA AGT TGG AAT TGA TGA AGT TGC TCT TGA G 3'
abi-1_A5_F	Forward	ABI-1(427-469)	5' GGG GAC AAC TTT GTA CAA AAA AGT TGG AAA ATG AAA GAA GAC GAG TTG ACA CTT CG 3'
abiRevatt ¹	Reverse	ABI-1(427-469)	5' GGG GAC AAC TTT GTA CAA GAA AGT TGG TAC TGG AAC TAC GTA GTT TCC AG 3'
abi-1_174-426_F	Forward	ABI-1(174-426)	5' GGG GAC AAC TTT GTA CAA AAA AGT TGG AAA ATG TCT GGC AGT TCT CCA TCA CAA T 3'
abi-1_174-426_R	Reverse	ABI-1(174-426)	5' GGG GAC AAC TTT GTA CAA GAA AGT TGG TGC AGC ATC ATA GTC GTA CAG G 3'
mig10aforatt ¹	Forward	MIG-10A	5' GGG GAC AAC TTT GTA CAA AAA AGT TGG AAA ATG GAC ACT TAC GAC TTC CCG 3'
mig10revatt ¹	Reverse	MIG-10A	5' GGG GAC AAC TTT GTA CAA GAA AGT TGG ACA CTC CAT GGT TGC CAT TTT CTC 3'

To introduce the coding sequence for each deletion mutant into a vector suitable for expression, 150 ng of each entry clone was recombined with 150 ng of either the pUAST-a-V5/6XHis or pUAST-a-GFP destination vector (provided by J. Duffy, Worcester Polytechnic Institute) by adding 2 μ L of LR Clonase II enzyme mix (Invitrogen) to each reaction and incubating for 1 hr.

at 25°C. 3 µL of each reaction was transformed into 50 µL Subcloning-Efficiency DH5α *E. coli* chemically competent cells (Invitrogen) and spread on LB-agar plates supplemented with 50 µg/µL ampicillin. Plates were incubated overnight at 37°C and colonies selected the following day to inoculate culture tubes of 5 mL liquid LB supplemented with 50 µg/µL ampicillin. Plasmid DNA was isolated as before using the QIAprep Spin Miniprep kit (Qiagen) and confirmed as the desired expression clone by restriction digest and sequencing analysis.

Constructs designed for expression of MIG-10A and MIG-10B in the *C. elegans* excretory cell were generated by directional cloning of *mig-10a* and *mig-10b* cDNA into the pVA700 vector (provided by E. Stringham, Trinity Western University). A summary of this process is shown in Figure 8. Primers were designed to flank the 5' and 3' ends of each cDNA with PstI and KpnI sites, respectively (Table 2). PCR products were generated using 4 ng of the appropriate template, 20 pmol of each primer, and 5 units of ExTaq polymerase (TaKaRa). The presence and expected size of each product were confirmed on a 0.8% agarose gel in TAE buffer and products were gel purified using the QIAquick Gel Extraction kit (Qiagen). Purified PCR products were then ligated into the pGEM-T Easy Vector (Promega) using the accompanying kit. 4 µL of each ligation was transformed into 50 µL of Max-Efficiency DH5α *E. coli* chemically competent cells (Invitrogen) and cells were spread on LB+agar plates supplemented with 50 µg/µL ampicillin and incubated overnight at 37°C. Selected colonies were then grown overnight at 37°C in liquid LB supplemented with 50 µg/µL ampicillin. Plasmid DNA was isolated using the QIAprep Spin Miniprep kit (Qiagen) and preps of vector containing an insert of the expected size were identified by restriction digest with KpnI and PstI. The cDNA insert in vectors confirmed by diagnostic digest were then verified by sequencing analysis. Coding sequences for *mig-10a* and *mig-10b* were then excised from the pGEM-T Easy Vector by digestion of miniprep DNA

with KpnI and PstI. Digested vector and insert were separated on a 0.8% agarose gel in TAE and cDNA inserts were purified using the QIAquick Gel Extraction kit (Qiagen). The pVA700 backbone was digested and purified in the same manner. Each cDNA insert was combined in a 3-fold molar excess with digested pVA700 and incubated for 3 hrs. at 16°C with 1 µL T4 DNA ligase (NEB). 4 µL of each ligation was transformed into 50 µL of Max-Efficiency DH5α *E. coli* chemically competent cells (Invitrogen) and cells were plated on LB+agar supplemented with 50 µg/µL ampicillin and incubated overnight at 37°C. Colonies were selected, grown in liquid LB medium, minipreped, and analyzed as previously described. Recombinant vectors containing the coding sequence for *mig-10a* and *mig-10b* in frame with the nucleotide sequence encoding GFP, termed pVA700-M10A and pVA700-M10B, respectively, were confirmed by sequencing analysis.

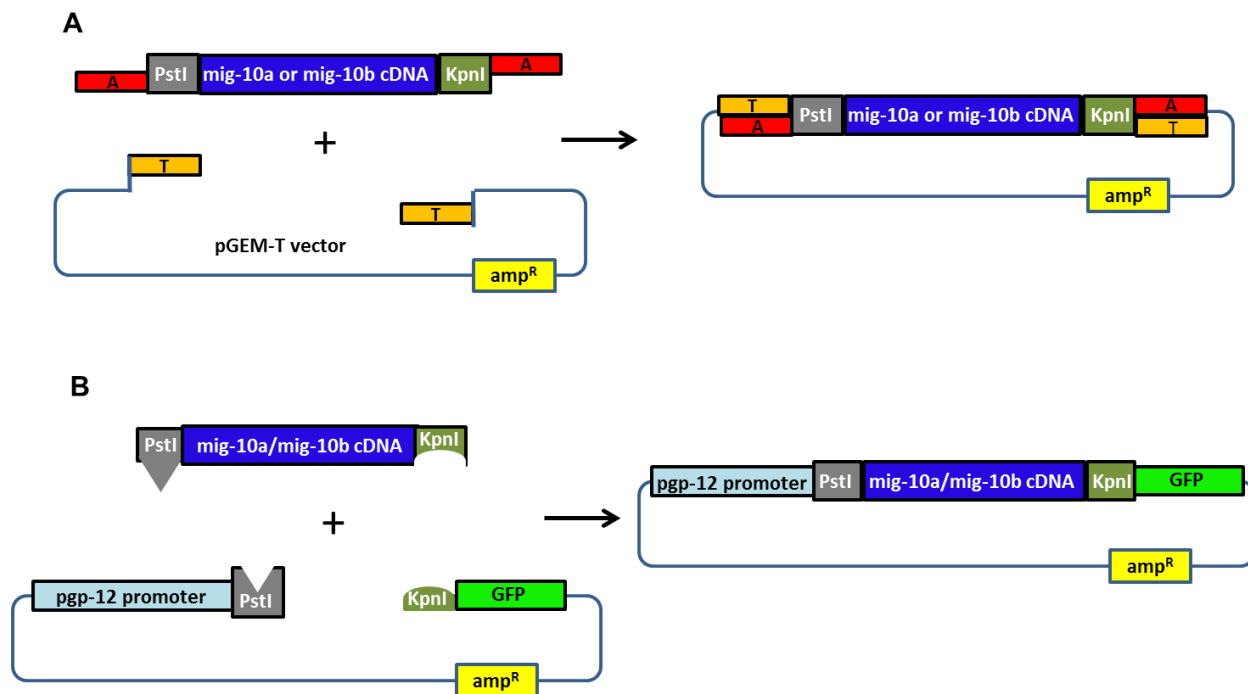


Figure 8: Summary of nematode expression vector cloning strategy. (A) Sequence encoding MIG-10A or MIG-10B was amplified by PCR with primers that introduced a PstI site to the 5' end of the start codon and a KpnI site 3' to the end of the coding sequence. Addition of a single deoxyadenosine to the 3' end of each strand of the PCR product by the polymerase allowed for ligation into the pGEM-T vector (Promega), which contained complementary deoxythymidine overhangs at the end of each 3' strand in the vector. (B) Digestion of the product of the ligation shown in (A) with PstI and KpnI allowed for isolation of the fragment containing the coding sequence of interest. This sequence could then be inserted in the proper orientation into digested pVA700.

Table 2: Primers used to generate amplicons for cloning of nematode expression vectors. The indicated primers were designed to amplify the coding sequences of mig-10a and mig-10b with a KpnI site adjacent to the 5' end of each sequence and a PstI site adjacent to the 3' end. Blue sequence: KpnI site; Red sequence: PstI site; Green sequence: nucleotides added to put GFP coding sequence in frame with the upstream coding sequence of each isoform.

Primer Name	Forward or Reverse	Compatible cDNA	Sequence
mig-10apVA700_F	Forward	mig-10a	5' GCG ATA CTG CAG ATG GAC ACT TAC GAC TTC CC 3'
mig-10bpVA700_F	Forward	mig-10b	5' GCG ATA CTG CAG ATG TAT CAC GAT CGA CGG C 3'
mig-10pVA700_R	Reverse	mig-10a and mig-10b	5' GCG ATA GGT ACC AT ACA CTC CAT GGT TGC CAT TTT CTC 3'

Microinjection and Rescue Experiments

Young adult hermaphrodites from the BW315 *mig-10(ct41)* strain were mounted in halocarbon oil on 2% agarose pads. The distal gonad of each animal was injected with one of the DNA mixtures shown in Table 3 under Nomarski optics (Fig. 9). Animals were recovered in M9 buffer and picked to individual NGM plates containing OP50 *E.coli* as a food source and grown at 20°C. Approximately 4 days post-injection, progeny (F1) were examined under a stereoscope for fluorescence of the RFP coelomocyte marker. Progeny expressing this injection marker were picked to individual plates and incubated at 20°C. Descendants of these animals were examined for expression of the coelomocyte marker. A line was established for each F1 that produced transformed descendants. GFP fluorescence was not observed in any of the established lines, so several MIG-10AB, MIG-10A, and MIG-10B lines were crossed with a line stably expressing the *pgp-12::GFP* marker to mark the excretory cell. The lengths of the posterior and anterior excretory canals of L4 animals from one resulting line of each genotype were measured and normalized to the body length of each animal. Measurements of excretory canal length were also performed on wild type and *mig-10(ct41)* animals carrying the *pgp-12::GFP* transgene to mark the excretory cell. Siblings, which are animals descended from transformants that have lost the rescuing DNA or “array”, were also analyzed as an additional negative control. Statistical analysis was then performed to compare the mean anterior and posterior excretory canal lengths of these groups. All crosses with the line carrying the *pgp-12::GFP* marker and subsequent analysis were performed by M. Kuhlwein (Hashmi and Kuhlwein, 2011).

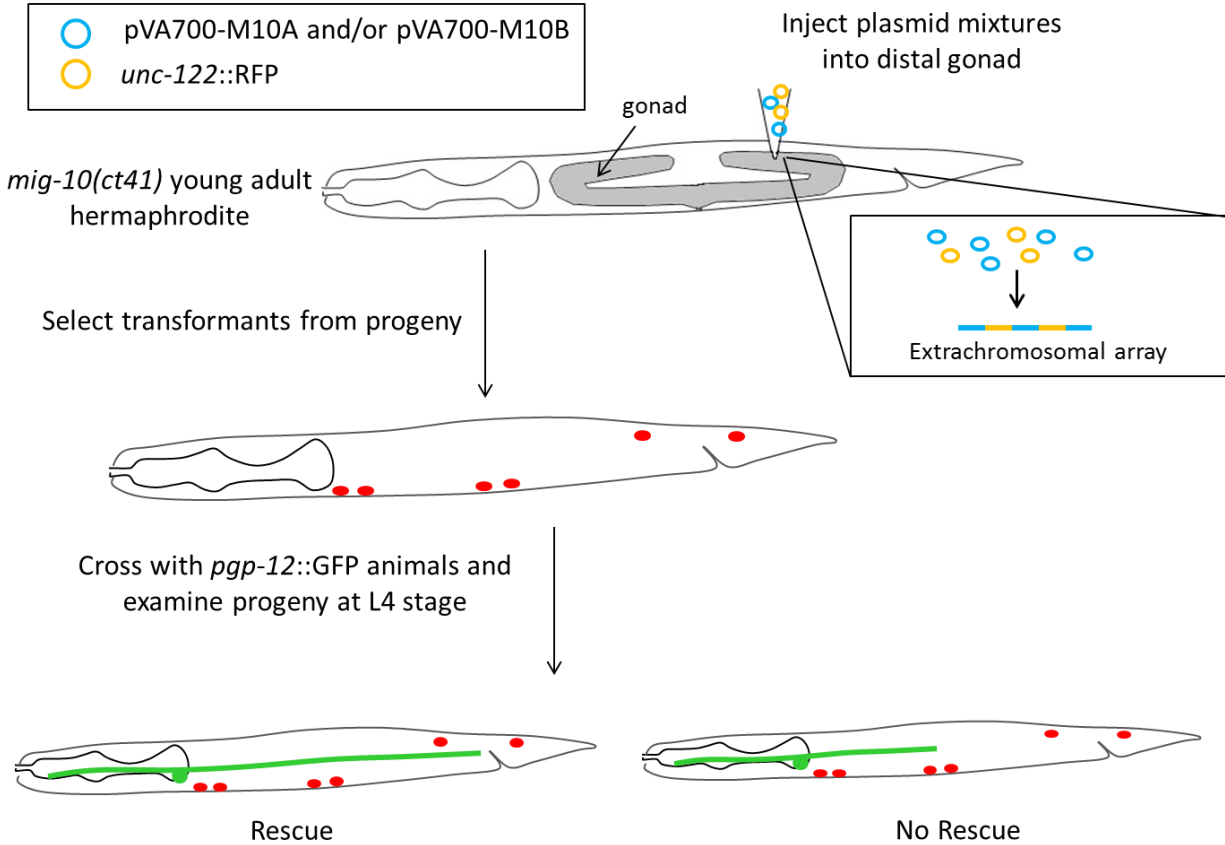


Figure 9: Overview of microinjection and transformation procedure. Mixtures of constructs expressing either MIG-10A or MIG-10B specifically in the excretory cell and the coelomocyte marker *unc-122::RFP* were injected into the distal gonad of *mig-10(ct41)* young adult hermaphrodites. Variable amounts of each injected plasmid randomly assemble into arrays, which are incorporated into cells as they undergo oogenesis. Progeny transformed with arrays were selected based on expression of the coelomocyte marker and then crossed to animals from the *pgp-12::GFP* strain. Progeny from these crosses were analyzed at the L4 stage to determine the extent of rescue of excretory canal truncation. Crosses and analysis of excretory canal length were performed by M. Kuhlwein.

Table 3: DNA mixtures used for microinjection. Expression constructs were combined in dH₂O to create mixtures of the indicated concentrations of each construct. RFP expression in the coelomocytes directed by the *unc-122::RFP* construct was used for positive selection of transformants.

Injection Mixture	<i>unc-122::RFP</i> (ng/ μ L)	pVA700-M10A (ng/ μ L)	pVA700-M10B (ng/ μ L)
A	40	160	0
B	40	0	160
AB	40	80	80

Cell Culture and Protein Expression

Cells from the embryonic *D. melanogaster* S3 line (provided by J. Duffy, Worcester Polytechnic Institute) were maintained at room temperature in Schneider's 1X Drosophila medium (Gibco) + 12.5% FBS (Valley Biomedical). Cells were diluted 1:10 (v:v) when confluent (about every 4 days). To prepare cells for transfection, 2 mL of a 1:10 (v:v) dilution of confluent cells was used to seed each well of one or more 6-well plates. When cells reached approximately 90% confluence (about 2-3 days after seeding), co-transfection of 133 ng Arm-GAL4 (provided by J. Duffy, Worcester Polytechnic Institute) and 133 ng of each of the appropriate expression construct(s) was performed using Effectene reagent (Qiagen). Cells were harvested 4 days post-transfection for use in the immunoprecipitation system.

Immunoprecipitation and Western Blotting

Each sample of transfected S3 cells (1 well of cells from a 6-well plate) was resuspended in 2.2 mL of Schneider's + 12.5% FBS by pipetting and 75 μ L was removed for the whole cell lysate (WCL) sample. Cells in WCL samples were pelleted by centrifugation at 8,000 rpm in a microcentrifuge for 5 min., resuspended in 50 μ L 1X sample buffer (12 mM Tris-HCl, pH 6.8; 5% glycerol; 0.4% SDS; 2.88 mM β -mercaptoethanol; 0.02% bromophenol blue) by briefly vortexing, and stored at -20°C. The cells remaining for each sample were pelleted by centrifugation at 2,000 rpm in a table top centrifuge for 2 min. and resuspended by brief vortexing in 1 mL of Lysis Buffer {50mM Tris, pH 8; 150 mM NaCl; 2 mM EDTA; 0.5% NP-40; 2X protease inhibitor cocktail (Complete, EDTA-free, Roche); 1X phosphatase inhibitors (1 mM Na₃VO₄; 5 mM Na₄P₂O₇; 5 mM NaF)}. Lysates were incubated on ice for 15 min. and the insoluble fraction was then removed from each by centrifugation at 14,000 rpm in a microcentrifuge for 15 min. at 4°C. Each sample was then incubated overnight at 4°C with 2 μ L

anti-GFP antibody (rabbit polyclonal, Clontech). 70 μ L/sample of a 10% (w:v) slurry of protein A sepharose (PAS; GE Healthcare) in a solution of 20% ethanol and 80% TBS (v:v) was washed overnight at 4°C in a 24-fold volumetric excess of PAS wash buffer (50 mM Tris, pH 8; 200 mM glycine; 1% Tween-20). The PAS slurry was pelleted by centrifugation at 500 rpm in a table top centrifuge for 3 min. at 4°C and washed 3X in 1 mL Lysis Buffer without protease or phosphatase inhibitors. resuspended in an equal volume of Lysis Buffer. 50 μ L of this slurry was added to each lysate + antibody sample and incubated for 2 hr. at 4°C with constant, gentle shaking. The PAS from each sample was then washed 3X in 1 mL Buffer X (50 mM Tris, pH 8.5; 250 mM NaCl; 2 mM EDTA; 1% NP-40) with pelleting of the PAS by centrifugation at 1,000 rpm in a microcentrifuge for 20 sec. at 4°C between washes. Each sample was then washed 1X in 50 mM Tris, pH 8. As much buffer as possible was then removed from each PAS sample. To each sample, 25 μ L of 2X Sample Buffer was added and samples were boiled for 5 min. WCL samples were boiled for 6 min. All samples were cooled to room temperature and briefly centrifuged at top speed in a microcentrifuge to collect the condensate.

From each of the IP and WCL samples, 15 μ L was removed and separated on a 10% polyacrylamide gel under 20 mA constant current. Proteins were transferred to nitrocellulose membranes (GE Healthcare) under a constant voltage of 100V for 1 hr. Membranes were Ponceau stained and blocked for 1 hr. at room temperature in 5% (w:v) non-fat dry milk (NFDM) in TBST (20 mM Tris, pH 7.6; 150 mM NaCl; 0.1% Tween-20). Membranes were then incubated overnight at 4°C in 1:5,000 (v:v) dilutions of anti-V5 antibody (mouse monoclonal, Invitrogen) in a 1% (w:v) solution of NFDM in TBST. Membranes were washed 5X in TBST for 5 min. per wash and then incubated for 1 hr. at room temperature in 1:20,000 (v:v) dilutions of HRP-conjugated antibody (goat anti-mouse, Jackson Immuno Research) in 5% (w:v) NFDM in

TBST. Membranes were washed 5X in TBST, incubated for 10 min. in HRP substrate working solution (Universal His Western Blot kit 2.0, Clontech or SuperSignal West Femto, Pierce), and exposed to film optimized for chemiluminescent detection (Roche).

Subsequent detection of GFP-tagged constructs was performed by stripping membranes according to the GE Healthcare protocol. Membranes were then blocked as before and incubated overnight at 4°C in 1:1,000 (v:v) dilutions of anti-GFP antibody (mouse monoclonal JL-8, Clontech) in a 0.5% (w:v) solution of NFDm in TBST. The remaining steps in the detection process were performed as before. The immunoprecipitation procedure is summarized in Figure 10.

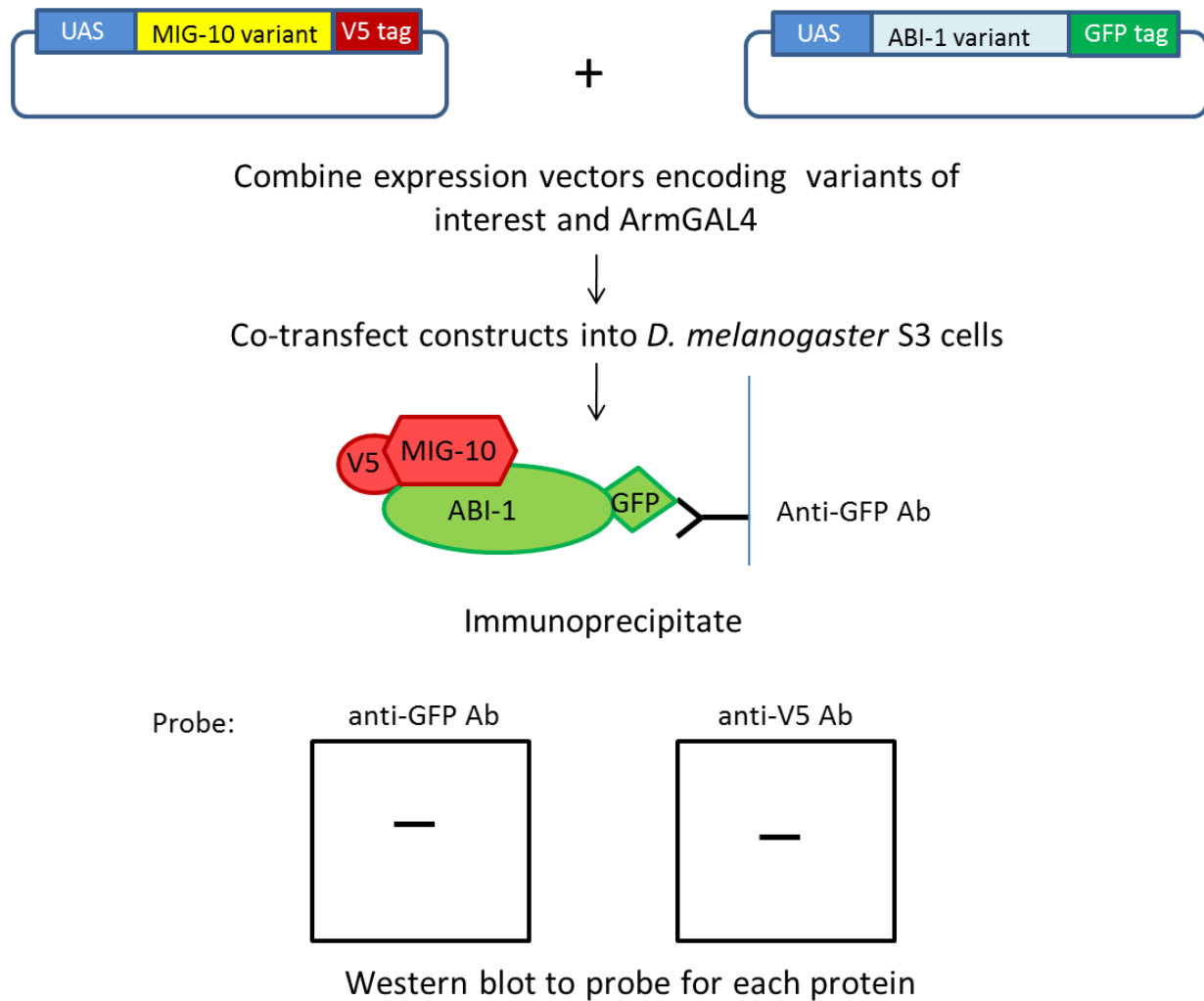


Figure 10: Overview of immunoprecipitation analysis. Variants of interest were co-transfected with ArmGAL4 in S3 cells. Immunoprecipitations were performed with an anti-GFP antibody 4 days after transfection. Blots of immunoprecipitates were probed first with anti-V5 antibody to assess co-immunoprecipitation and were then reprobed with an antibody against GFP.

The conditions for the immunoprecipitation assay seemed optimal for some time, but then continued to yield blots in which the signal was weak or undetectable. Components of the experimental system were then varied individually to determine if alteration could improve the assay. The first of these optimization experiments was designed to compare the pre-existing supply of anti-V5 antibody with that of a fresh stock from Invitrogen. To do so, two wells on a

10% polyacrylamide gel were each loaded with 15 μ L from the same WCL sample containing MIG-10A::V5. Proteins were separated on these gels by electrophoresis and transferred to a nitrocellulose membrane as previously described. The lanes on the membrane were then cut and developed in separate 1:5,000 dilutions of anti-V5 antibody, with one strip receiving fresh antibody and the other receiving antibody from the pre-existing stock. The remainder of the detection process was performed as previously described for each strip, and signal detected from each membrane strip was compared. Similar experiments in which only the experimental condition of interest was altered were conducted to compare the following: fresh vs. pre-existing stocks of both monoclonal and polyclonal anti-GFP antibody, fresh vs. pre-existing batches of PAS, fresh vs. pre-existing stocks of plasmid DNA, washed vs. unwashed PAS, fresh vs. pre-existing stocks of both protease and phosphatase inhibitor cocktails, and autoclaved vs. non-autoclaved stocks of Lysis Buffer (autoclaving was performed before addition of inhibitors) and Buffer X.

Results

The interaction between ABI-1 and MIG-10 observed in the yeast two-hybrid system (Gosselin and O'Toole, 2008) is hypothesized to contribute to the regulation of actin remodeling events critical for cell and process migration. One prediction of this hypothesis is that MIG-10 and ABI-1 have overlapping patterns of expression *in vivo* such that they are capable of coming into physical contact. Excretory canal outgrowth is disrupted in *mig-10* and *abi-1* mutants (Manser and Wood, 1990; Schmidt *et al.*, 2009; Grant and Dubuke, 2009), suggesting MIG-10 and ABI-1 function in a common pathway to direct development of these canals. It has been suggested that ABI-1 functions in a cell autonomous fashion in the excretory cell during canal outgrowth (Schmidt *et al.*, 2009), which would suggest that MIG-10 is also likely to function in a cell autonomous fashion during this process. To test this prediction, expression of MIG-10 was confined to the excretory cells of *mig-10(ct41)* animals. Rescue of excretory canal truncation in these animals would be indicative of a cell autonomous role for MIG-10 in canal development and would suggest MIG-10 and ABI-1 could function in a common pathway in this cell.

Prior analysis of excretory canal development in *mig-10(ct41)* animals treated with *abi-1(RNAi)* demonstrated that canal truncation is more severe in these animals than in *mig-10(ct41)* animals or *abi-1(RNAi)*-treated animals (Grant and Dubuke, 2009). Enhancement of this phenotype is inconsistent with a model in which MIG-10 and ABI-1 function in a single, linear pathway. In light of the results of yeast two-hybrid analysis, this enhancement suggests that these proteins either have some functions in excretory canal development that are non-overlapping or that the result of the yeast two-hybrid screen is an artifact of the system. To distinguish between these possibilities, the interaction between MIG-10 and ABI-1 was re-examined using a co-immunoprecipitation system.

Autonomous expression of MIG-10A or MIG-10B in the excretory cell partially rescues excretory canal truncation in *mig-10(ct41)* animals

MIG-10 isoform expression requirements for excretory canal outgrowth were previously investigated using fosmids. *mig-10(ct41)* animals carrying a fosmid from which only MIG-10A and MIG-10B were expressed displayed wild type excretory canals, indicating MIG-10C is unnecessary for excretory canal outgrowth (Fig. 11; Zhang, 2010). Fosmids are constructed with genomic DNA, so expression of MIG-10A and MIG-10B was driven by the endogenous promoters in this analysis. This precluded the identification of a single cell or subset of cells in which expression of MIG-10 is sufficient for rescue of the excretory canal truncation phenotype of *mig-10(ct41)* animals.

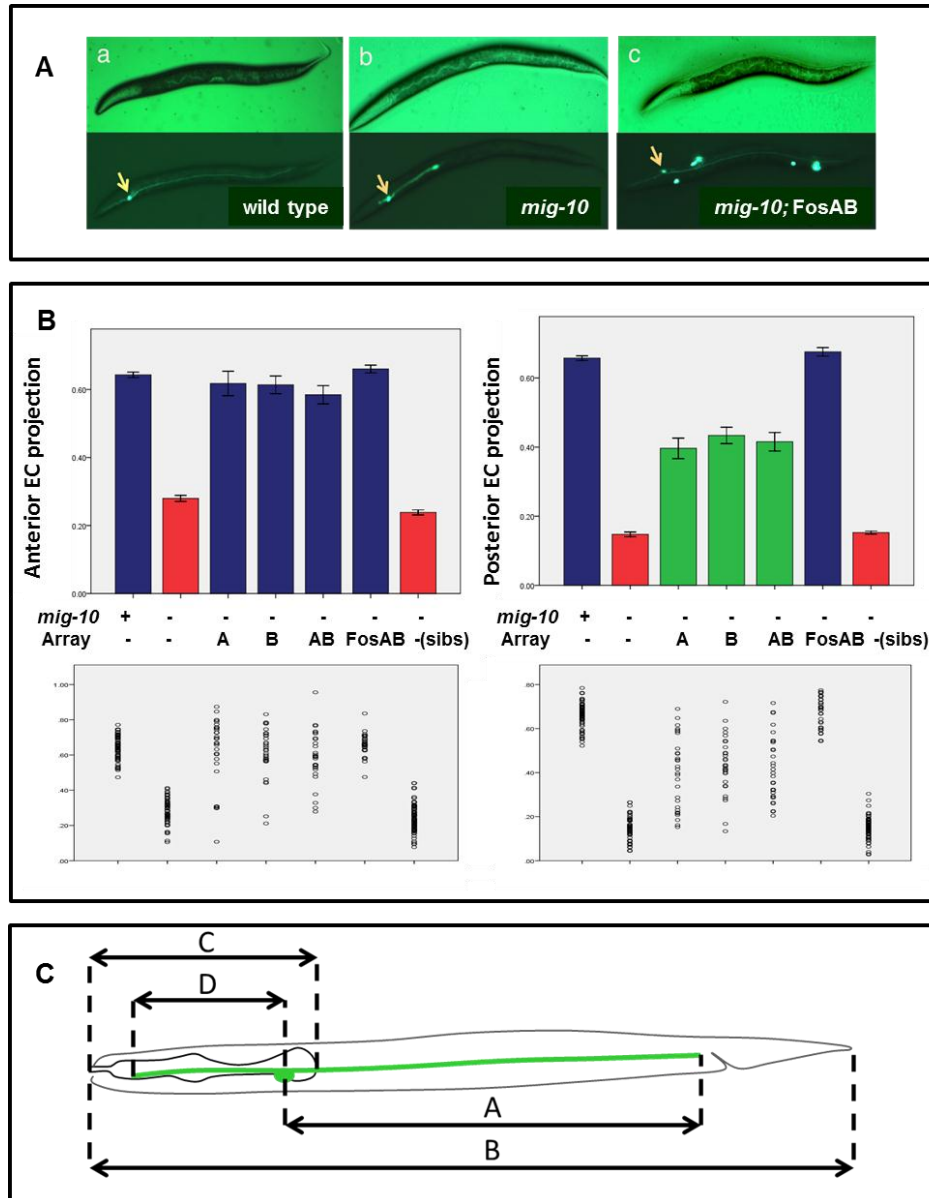


Figure 11: Cell autonomous expression of either MIG-10A or MIG-10B in the excretory cell rescued anterior canal truncation and partially rescued posterior canal truncation. (A) Excretory cell visualization by GFP fluorescence in animals of the indicated genotype. (B) Upper panels: comparison of mean anterior and posterior excretory canal lengths in animals of the indicated genotype at the L4 stage. A=MIG-10A array, B=MIG-10B array, AB=MIG-10AB array, sibs=siblings. Error bars, ± 1 SE. $n \geq 40$ animals per genotype. Genotypes depicted in the same color are not significantly different while those of different color are significantly different ($p < 0.05$, ANOVA, Tukey HSD post-hoc tests). Lower panels: excretory canal measurements for each individual observed in each genotype are shown as single dots. (C) Measurements of anterior excretory canal length were normalized by the distance from the tip of the head to the end of the posterior bulb of the pharynx (D/C) while measurements of posterior excretory canal length were normalized by the body length of the nematode (A/B). Measurements and statistical analysis of FosAB, wild type, *mig-10(ct41)*, and sibling animals were performed by S. Zhang (Zhang, 2010) while measurements and statistical analysis of animals carrying arrays and siblings was performed by M. Kuhlwein (Hashmi and Kuhlwein, 2011).

In light of the results of the fosmid analysis, the simplest model for excretory cell outgrowth is one in which autonomous expression of MIG-10A and MIG-10B in the excretory cell alone is sufficient for canal outgrowth. To test this model, nine *pgp-12::MIG-10AB::GFP* lines were established. GFP fluorescence was not detected in the excretory cells of any animals from these lines, so several were crossed with a line stably expressing the *pgp-12::GFP* marker and one of the resulting lines was analyzed. The mean length of the anterior excretory canal for this *pgp-12::MIG-10AB::GFP* line was not significantly different from that of wild type animals or animals carrying the MIG-10AB fosmid (FosAB). However, the mean anterior excretory canal length of each of these groups was significantly greater than the mean lengths of *mig-10* mutant animals or siblings. Comparison of the mean posterior excretory canal lengths among these groups demonstrated that animals carrying the *pgp-12::MIG-10AB::GFP* array were significantly different both from wild type animals and *mig-10* mutants and siblings. Thus, autonomous expression of MIG-10A and MIG-10B exclusively in the excretory cell of *mig-10(ct41)* animals completely rescued anterior excretory canal truncation and partially rescued posterior excretory canal truncation (Fig. 11).

Although these results established a cell autonomous function for MIG-10 in promoting excretory canal outgrowth, they did not indicate whether both MIG-10A and MIG-10B function in this manner or if only one of these isoforms was responsible for the observed partial of the excretory canals. To better characterize the contribution of each isoform to the observed partial rescue, two lines carrying *pgp-12::MIG-10A::GFP* arrays and two carrying *pgp-12::MIG-10B::GFP* arrays were established and one line of each type was crossed with a line stably expressing the *pgp-12::GFP* marker. Analysis and comparison of the resulting lines revealed that no significant difference existed between animals carrying the MIG-10A array and those

carrying MIG-10B array with respect to mean anterior and mean posterior excretory canal lengths. Both groups displayed the same extent of rescue of the anterior and posterior excretory canals as had been previously observed in animals carrying the MIG-10AB array (Fig.11). These data demonstrate that MIG-10A and MIG-10B act redundantly to promote excretory canal outgrowth in a cell autonomous fashion.

Animals carrying any of these three arrays were also similar in that the variability in the extent of rescue was much greater for each of these groups than it was for wild type, *mig-10(ct41)*, or FosAB animals (Fig. 11, lower panels). Some animals from each of the *pgp-12::MIG-10AB::GFP*, *pgp-12::MIG-10A::GFP*, and *pgp-12::MIG-10B::GFP* lines showed complete rescue of the anterior and posterior excretory canals while in other animals, the excretory cell canals were as truncated as in *mig-10(ct41)* animals or siblings. None of the FosAB animals examined displayed excretory canals that were as truncated as those of *mig-10(ct41)* animals or siblings. Thus, FosAB animals differ from animals carrying one of the three arrays in terms of the variability in extent of rescue.

MIG-10A interacts with ABI-1 through either the ABI-1 N-terminus, SH3 domain, or both of these regions

The establishment of cell autonomous functions for MIG-10A and MIG-10B in the excretory cell, in which ABI-1 also functions cell autonomously (Schmidt *et al.*, 2009), suggests that these proteins are expressed together in this cell *in vivo*. To further examine the potential of these proteins to physically interact, an insect cell expression system was used to continue the analysis initiated with the yeast two-hybrid system. Briefly, vectors suitable for GAL4-induced expression in *D. melanogaster* S3 cells were generated using the Gateway cloning system such that full length ABI-1 and ABI-1 deletion mutants were fused to GFP tags whereas MIG-10A,

MIG-10B, and MIG-10 deletion mutants were fused to V5 tags (Fig. 12). Vectors encoding GFP- and V5- tagged variants were then co-transfected pairwise into S3 cells along with a vector encoding a ubiquitously expressed GAL4 fusion protein. Immunoprecipitations of ABI-1 variants from the lysates of these cells were performed and then analyzed by western blotting using an anti-V5 antibody.

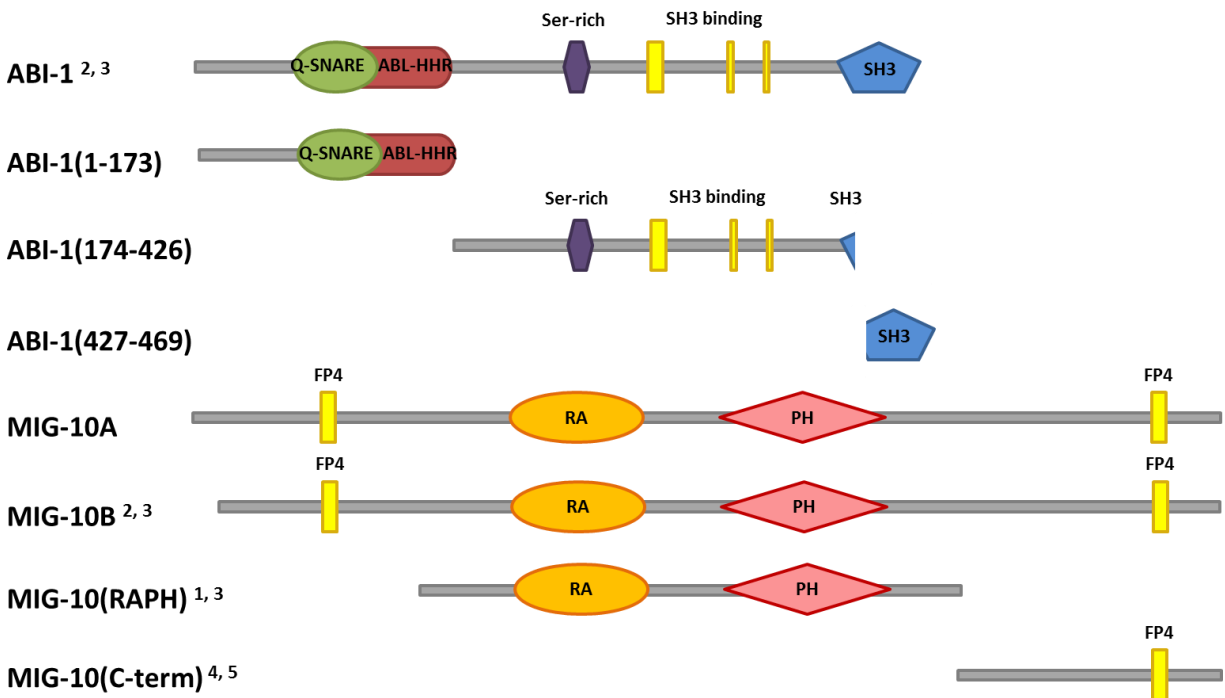


Figure 12: Variants of MIG-10 and ABI-1 examined in the co-immunoprecipitation system. ABI-1 variants were tagged at the C-terminus with GFP and MIG-10 variants were tagged at the C-terminus with V5/6XHis, but for simplicity, tags are not shown. Cloning to generate entry and expression clones encoding these variants was performed using the Gateway system.

- ¹ Entry clone generated by S. Zhang
- ² Entry clone generated by T. Grant and M. Dubuke
- ³ Expression clone generated by S. Zhang
- ⁴ Entry clone generated by K. Milligan
- ⁵ Expression clone generated by K. Milligan

Using this method, MIG-10A::V5 was detected in the immunoprecipitate from cells co-expressing MIG-10A::V5 and ABI-1::GFP but was not detected in the immunoprecipitate from

cells expressing MIG-10A::V5 alone (Fig. 13), indicating MIG-10A::V5 is not retained nonspecifically during the immunoprecipitation. Prior investigation of the abilities of various ABI-1 deletion mutants to interact with MIG-10A in a yeast two-hybrid system showed that a mutant comprising residues 174 to 427 was incapable of robust interaction with MIG-10A, suggesting the N-terminus and C-terminal SH3 domain of ABI-1 were both required for robust interaction with MIG-10A (K. Schmidt, personal communication). To re-examine the contributions of these regions to the interaction between MIG-10A and ABI-1, a deletion mutant of ABI-1 lacking the N-terminus and most of the SH3 domain, termed ABI-1(174-426)::GFP, was co-expressed with MIG-10A::V5. Immunoprecipitation of ABI-1(174-426)::GFP from the lysates of these cells was performed alongside immunoprecipitation of ABI-1::GFP from the lysates of cells co-expressing ABI-1::GFP and MIG-10A::V5. Immunoprecipitation of ABI-1(174-426)::GFP in this manner repeatedly resulted in the isolation of much less MIG-10A::V5 than was isolated in the immunoprecipitates from cells co-expressing ABI-1::GFP and MIG-10A::V5 (Fig. 13). Similar outcomes were observed upon 5 repetitions of this experiment. Together these results demonstrate that co-immunoprecipitation of MIG-10A::V5 is specific to the full length variant of ABI-1::GFP and thereby confirm the interaction between MIG-10A and ABI-1 originally observed in the yeast two-hybrid system.

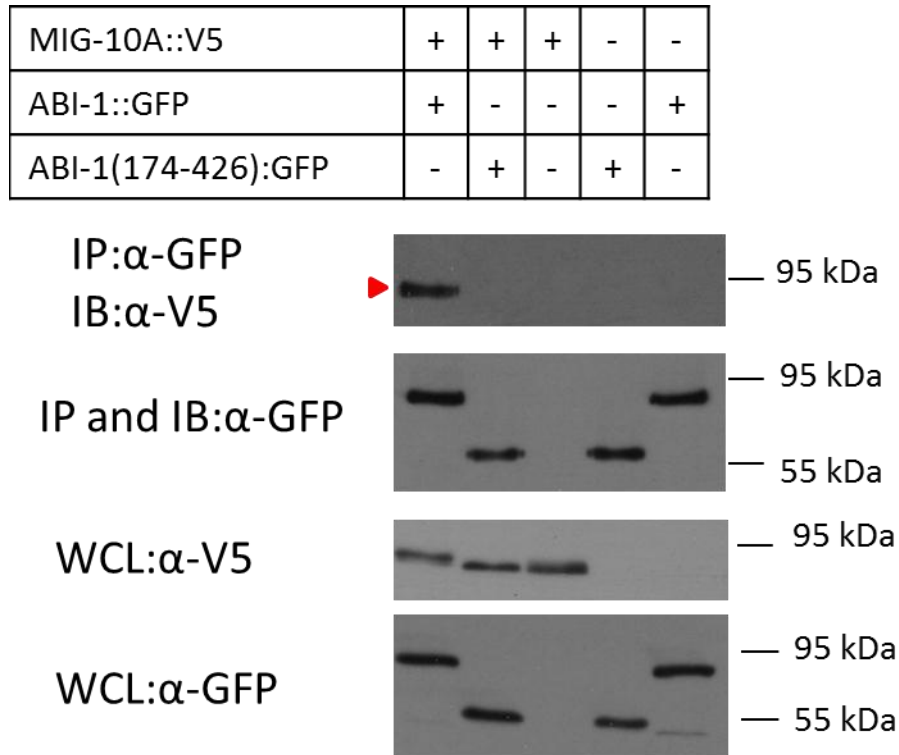


Figure 13: MIG-10A::V5 interacts with ABI-1::GFP but not with ABI-1(174-426)::GFP, a deletion mutant lacking the N-terminus and most of the SH3 domain. Expression clones were transfected into *D. melanogaster* S3 cells as indicated. Cells were lysed and immunoprecipitations were performed using an anti-GFP antibody. Immunoprecipitates were then analyzed by western blotting with the antibodies indicated on the left. MIG-10A::V5 co-immunoprecipitated with ABI-1::GFP (red arrow) but not with ABI-1(174-426)::GFP even though approximately equal amounts of ABI-1::GFP and ABI-1(174-426)::GFP were immunoprecipitated.

Another implication of the results of this experiment is that one or both of the regions the ABI-1(174-426)::GFP variant lacks, the N-terminus or SH3 domain of full length ABI-1, mediate the interaction with MIG-10A. To determine if only one of these regions is required for interaction with MIG-10A, ABI-1(1-173)::GFP and ABI-1(427-469)::GFP, which encode the ABI-1 N-terminus and SH3 domain, respectively, were each co-expressed with MIG-10A::V5 in S3 cells. Immunoprecipitations were then performed as before. Preliminary results show that MIG-10A::V5 co-immunoprecipitates with ABI-1(427-469)::GFP (Fig. 14) but not with ABI-1(1-

173)::GFP (Fig. 15), which suggests that the SH3 domain of ABI-1 may be the only region of this protein that mediates the interaction with MIG-10A.

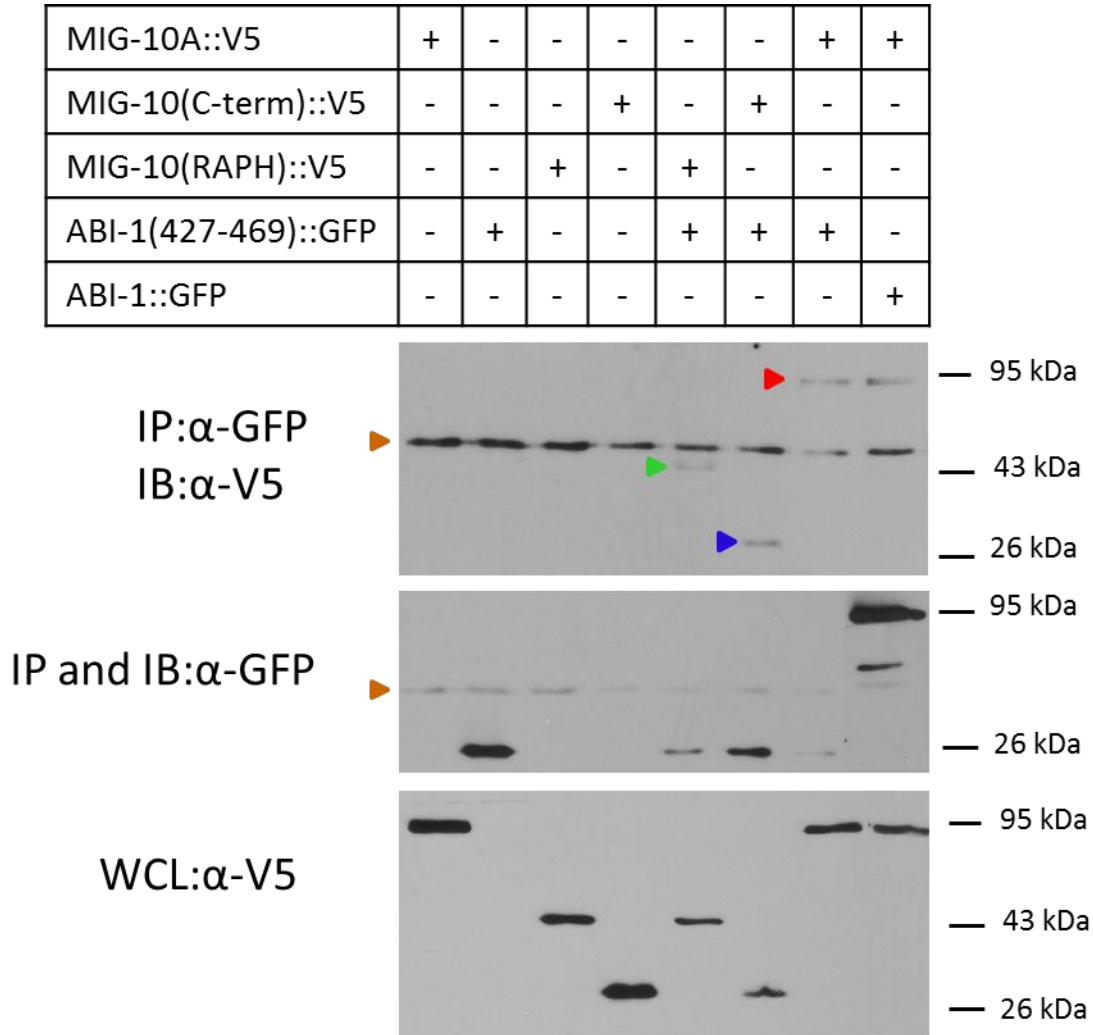


Figure 14: ABI-1(427-469)::GFP, a variant containing only the SH3 domain, interacts with MIG-10A::V5, MIG-10(C-term)::V5, and MIG-10(RAPH)::V5. S3 cells expressing the indicated constructs were lysed and immunoprecipitations were performed using an anti-GFP antibody. Analysis of the immunoprecipitates by western blotting with an anti-V5 antibody showed that MIG-10A::V5 (red arrow), MIG-10(RAPH)::V5 (green arrow), and MIG-10(C-term)::V5 (blue arrow) each co-immunoprecipitated with ABI-1(427-469)::GFP. S3 cells co-expressing MIG-10A::V5 and ABI-1::GFP were included as a positive control. Background was observed in all IP experiments from a protein of approximately 43 kDa (brown arrow) that was determined to originate from the PAS used in the immunoprecipitation experiments.

MIG-10A::V5	+	-	-	+	-	-	-
MIG-10(C-term)::V5	-	+	-	-	+	-	-
MIG-10(RAPH)::V5	-	-	+	-	-	+	-
ABI-1(1-173)::GFP	+	+	+	-	-	-	+

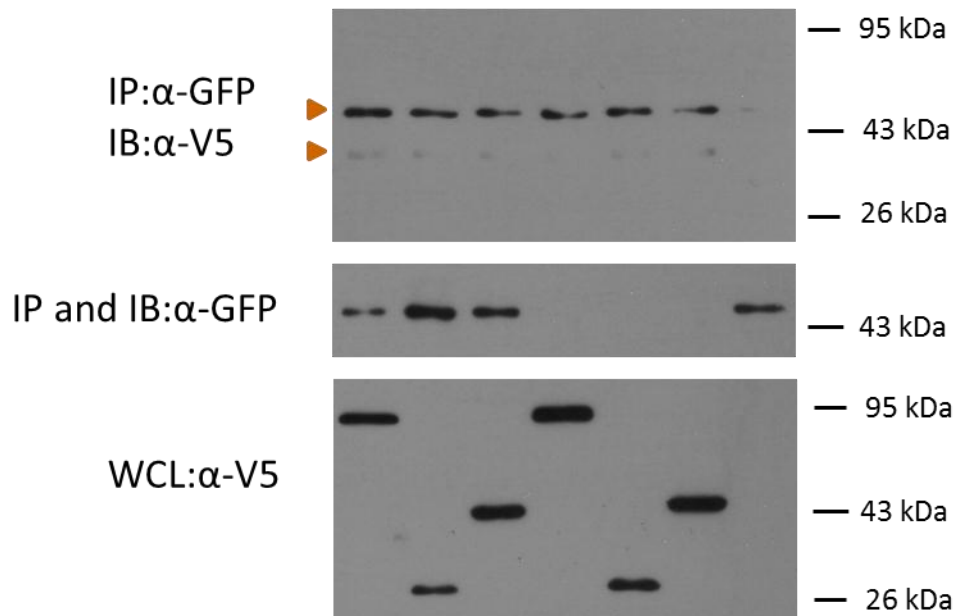


Figure 15: Neither MIG-10A::V5, MIG-10(C-term)::V5, or MIG-10(RAPH)::V5 interact with ABI-1(1-173)::GFP, the variant of ABI-1 containing only the N-terminus. S3 cells expressing the indicated constructs were lysed and immunoprecipitations were performed on the lysates with an anti-GFP antibody. Analysis of the immunoprecipitates by western blotting with an anti-V5 antibody showed that neither MIG-10A::V5, MIG-10(C-term)::V5, or MIG-10(RAPH)::V5 co-immunoprecipitated with ABI-1(1-173)::GFP (background is indicated by brown arrow).

Although these experiments cannot explore the possible *in vivo* significance of the interaction between MIG-10A and ABI-1, they have shed light on one possible consequence of the interaction. The band for MIG-10A::V5 in the V5-probed blot of the whole cell lysate (WCL) from MIG-10A::V5 and ABI-1::GFP co-transfected cells always appeared at a slightly higher position than the bands for MIG-10A::V5 observed in the WCL samples from MIG-10A::V5 and ABI-1(174-426)::GFP co-transfected cells and MIG-10A::V5 singly-transfected cells (Fig. 13,

third panel from top). The apparent decrease in the electromobility of MIG-10A::V5 correlates with co-expression of this protein with ABI-1::GFP and could be the result of a post-translational modification.

MIG-10B interacts with ABI-1

The possibility that multiple isoforms of MIG-10 could interact with ABI-1 had never been tested with the yeast two-hybrid system. To determine if MIG-10B could also interact with ABI-1, MIG-10B::V5 and ABI-1::GFP were co-expressed in S3 cells and ABI-1::GFP was immunoprecipitated from the lysate as before using a polyclonal anti-GFP antibody. An immunoprecipitation was also performed on the lysate of cells that only expressed MIG-10B::V5. When the immunoprecipitates were analyzed by western blotting with an anti-V5 antibody, MIG-10B::V5 was detected only in the immunoprecipitate from cells that had co-expressed MIG-10B::V5 and ABI-1::GFP (Fig. 16). These results were confirmed when this experiment was performed a second time (Fig. 17). Based on these results, the interaction originally observed between ABI-1 and MIG-10A in the yeast two-hybrid system is not isoform-specific with respect to MIG-10.

MIG-10A::V5	-	-	-	-	+	+
MIG-10B::V5	-	-	+	+	-	-
MIG-10(RAPH)::V5	+	+	-	-	-	-
ABI-1::GFP	-	+	-	+	-	+

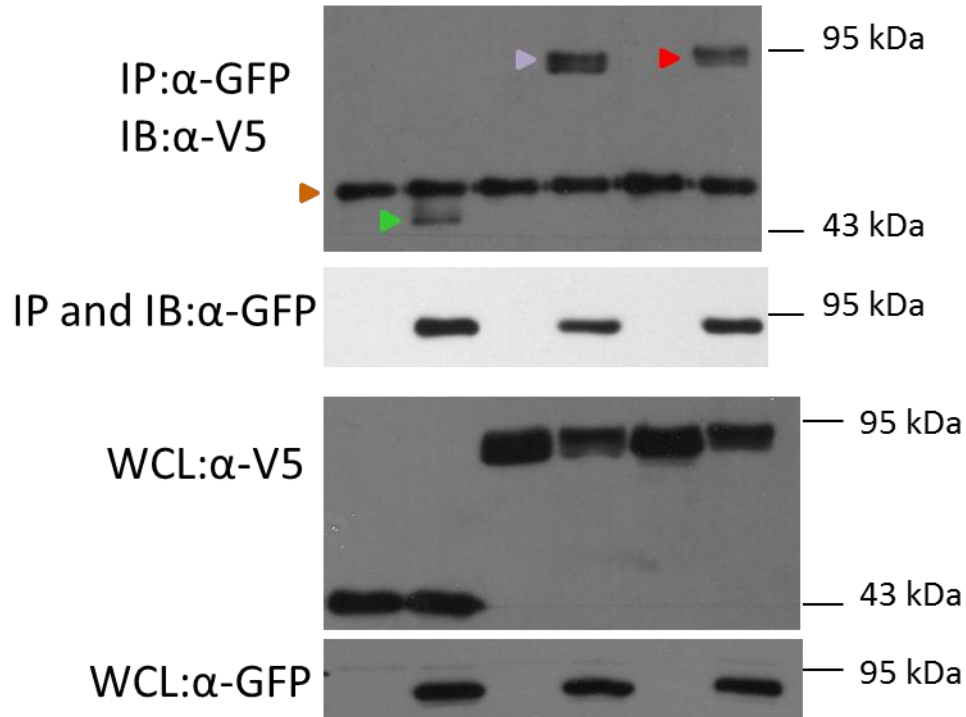


Figure 16: MIG-10B::V5 and MIG-10(RAPH)::V5 interact with ABI-1::GFP. S3 cells expressing the indicated constructs were lysed and immunoprecipitations were performed using an anti-GFP antibody. Analysis of the immunoprecipitates by western blotting with an anti-V5 antibody showed that MIG-10B::V5 (purple arrow) and MIG-10(RAPH)::V5 (green arrow) each co-immunoprecipitated with ABI-1::GFP. S3 cells co-expressing MIG-10A::V5 (red arrow) and ABI-1::GFP were included as a positive control. Background is indicated by the brown arrow.

MIG-10A::V5	+	-	-	+	-	-	-
MIG-10B::V5	-	+	-	-	+	-	-
MIG-10(C-term)::V5	-	-	+	-	-	+	-
ABI-1::GFP	+	+	+	-	-	-	+

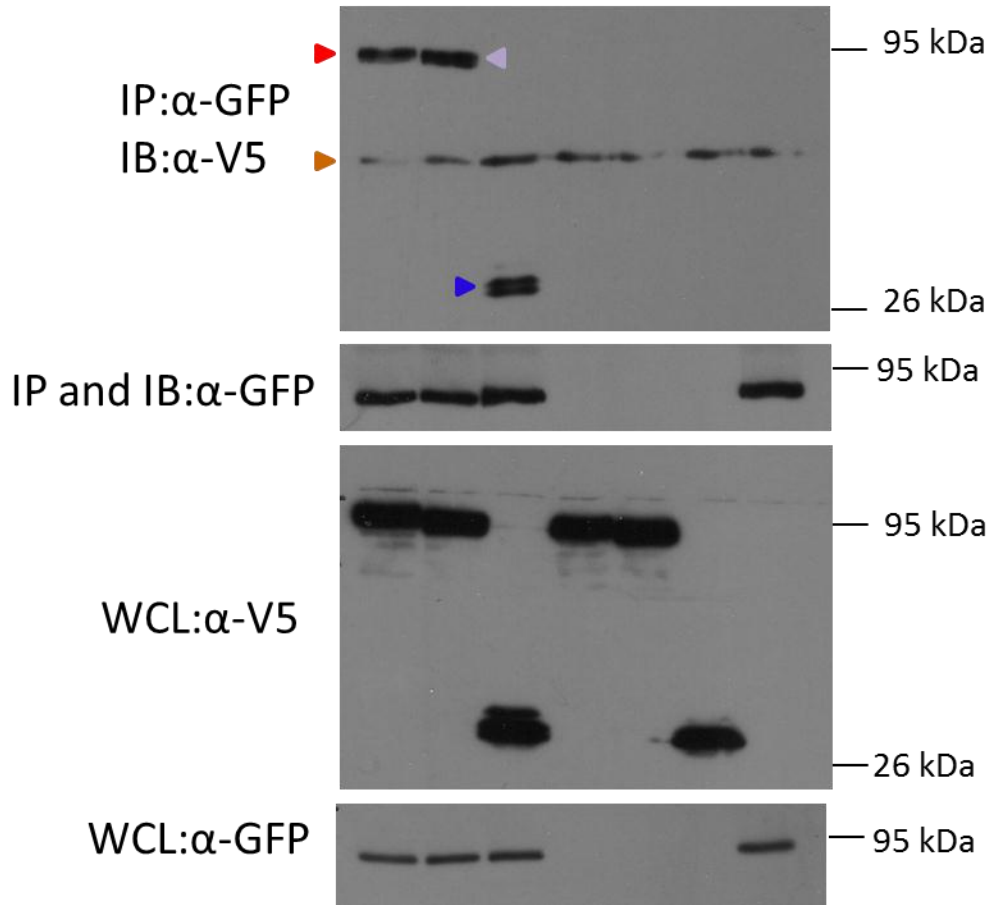


Figure 17: MIG-10B::V5 and MIG-10(C-term)::V5 interact with ABI-1::GFP. Immunoprecipitations with an anti-GFP antibody were performed on lysates of S3 cells expressing the indicated constructs. Both MIG-10B::V5 (purple arrow) and MIG-10(C-term)::V5 (blue arrow) co-immunoprecipitated with ABI-1::GFP. Cells co-expressing MIG-10A::V5 (red arrow) and ABI-1::GFP were used as a positive control. Background is indicated by the brown arrow.

The observation that two isoforms of MIG-10 interact with ABI-1 suggested that the ABI-1 binding site was likely in a region conserved in both isoforms. Since MIG-10A and MIG-10B

differ only in their N-termini, most of the amino acid sequence is conserved in these two isoforms. Two MIG-10 deletion mutants collectively span most of this common sequence: MIG-10(RAPH)::V5 encodes the central region of MIG-10 that includes the RA and PH domains while MIG-10(C-term)::V5 encodes the MIG-10 C-terminus. Each of these deletion mutants was co-expressed with ABI-1::GFP in S3 cells and immunoprecipitations were performed and analyzed as in previous experiments. Preliminary results suggest that both the MIG-10 C-terminus and the fragment encoding the RA and PH domains are capable of interacting with ABI-1 (Figs. 16 and 17). Consistent with these results, preliminary data also suggest these two variants of MIG-10 interact with ABI-1(427-469)::GFP but not with ABI-1(1-173)::GFP (Figs. 14 and 15). Taking all preliminary results into account, the co-immunoprecipitation analysis suggests that the SH3 domain of ABI-1 mediates an interaction with MIG-10A and MIG-10B through the C-terminus and central RAPH region of MIG-10 common to all isoforms.

Discussion

Cell and process migration are critical aspects of metazoan development, contributing not only to the development of single cells, such as the *C. elegans* excretory cell, but also to the formation of vast multicellular networks, such as the human brain. Underlying each of these morphological changes is the remodeling of the actin cytoskeleton at the leading edge, a complex process that is highly regulated by a plethora of secreted molecules and their associated signaling pathways. MIG-10 and ABI-1 are two adaptor proteins that participate in these pathways by relaying signals from the cell surface to proteins that directly modify actin assembly. The majority of research dedicated to these proteins has focused on each independently with little insight into how they, or the pathways of which they are a part, could potentially overlap. The results of this work confirm the finding of previous work in our laboratory suggesting that ABI-1 and MIG-10 physically interact. Furthermore, they demonstrate that MIG-10 can act cell autonomously to promote excretory canal outgrowth during *C. elegans* development. In light of recent evidence of a cell autonomous function for ABI-1 in promoting excretory canal outgrowth (Schmidt *et al.*, 2009), these results suggest MIG-10 and ABI-1 may function in a common pathway *in vivo*.

Further investigation is needed to determine where MIG-10 is expressed

Although autonomous expression of MIG-10 in the excretory cell can clearly drive canal outgrowth, whether or not this activity is normally relevant to excretory canal development cannot be determined without knowing if MIG-10 is expressed endogenously in the excretory cell. In order to address this question, the endogenous expression pattern of MIG-10 should be investigated more carefully using fluorescent reporters.

Expression of the MIG-10 fusions utilized in the rescue experiments described in this work also needs to be more carefully examined because fluorescence of the GFP tags was not observed. Fluorescence resulting from expression of the GFP coding sequence in the vector backbone was observed, indicating the original vector is functional. Sequence analysis revealed that within each rescuing vector, the C-terminal GFP tag is in frame with the coding sequence. One possible explanation for these results is that MIG-10A and MIG-10B are highly localized to the leading edge, and can therefore only be observed at the periphery of the excretory cell under higher magnification than was used in the course of these experiments. Re-examination of the strains used in these experiments is underway to evaluate this possibility. The protein levels of these isoforms could also be highly regulated so that once excretory canal outgrowth is complete in L4 animals, MIG-10A::GFP and MIG-10B::GFP exist at such low levels that they are undetectable by microscopy. Alternatively, detectable levels of these fusions may exist in animals at this stage, but misfolding of the GFP tags may prevent fluorescence. One means of determining if this is in fact occurring, and that the translation of the correct reading frame in each vector is taking place, would be to probe western blots of nematode lysates prepared from the transformed strains with an anti-GFP antibody. Detection of bands of the appropriate sizes for the MIG-10A and MIG-10B fusions would assure that expression is taking place, but is not detectable by microscopy.

If misfolding of MIG-10A::GFP and MIG-10B::GFP is confirmed, it could potentially explain why complete rescue of the anterior excretory canals was observed while only partial rescue was observed for the posterior canals. Normally, the posterior excretory canals extend a greater distance than the anterior canals and are consequently longer. If MIG-10 fusions expressed in the excretory cell are misfolded, their functionality may be decreased such that they retain some

ability to promote outgrowth, but not to the same extent as when properly folded. Thus, decreased outgrowth-promoting activity would be more apparent in the posterior excretory canals than in the anterior canals because the posterior canals must extend over a greater distance.

MIG-10 may act both cell autonomously and cell nonautonomously during excretory canal outgrowth

UNC-34, a component of the MIG-10 pathway, is known to contribute to excretory canal outgrowth (Hedgecock *et al.*, 1987). It seems likely UNC-34 functions cell autonomously in this process since it is known to function cell autonomously during CAN cell migration (Fleming *et al.*, 2010). Prior investigation of MIG-10 function during axon outgrowth demonstrated that it functions cell autonomously during this process (Quinn *et al.*, 2006). These data, along with the current model for MIG-10 function at the molecular level, suggest that MIG-10 is also likely to function cell autonomously in the excretory cell during canal development, even though expression of MIG-10 within this cell has yet to be demonstrated. Surprisingly, a previously conducted mosaic analysis suggests that MIG-10 is only required cell nonautonomously with respect to the excretory cell for canal outgrowth. While the data presented in this work clearly demonstrate that cell autonomous expression of MIG-10 in the excretory cell can rescue canal truncation, they do not rule out the possibility that MIG-10 also has a cell non-autonomous function during canal development.

In 1997, Manser, Roonprapunt, and Margolis conducted a mosaic analysis that suggested that autonomous expression of MIG-10 in the excretory cell is neither necessary nor sufficient for normal canal development. Animals carrying mutations in *mig-10* and *ncl-1* were transformed with a chromosomal duplication carrying wild type alleles of both genes. Unstable mitotic

transmission of the duplication resulted in the formation of mosaics. Inheritance of the duplication could be assessed with Nomarski optics for each cell based on the Ncl-1 phenotype, as mutation of *ncl-1* is characterized by an enlarged nucleolus. A class of 42 mosaics was identified for which the excretory canals were truncated. Among these animals, 29 had *mig-10(-)* excretory cells based on the Ncl-1 phenotype while the remaining 13 had *mig-10(+)* excretory cells. The finding that some animals had *mig-10(+)* excretory cells in which the canals were truncated suggested that cell autonomous expression of MIG-10 in the excretory cell is not sufficient for rescue of canal truncation. In addition, 5 ‘exceptional mosaics’ were identified that were superficially wild type with *mig-10(-)* excretory cells displaying canals that were as long or nearly as long as those of wild type animals. These observations provided the basis for the conclusion that autonomous expression of MIG-10 in the excretory cell is unnecessary for canal development (Manser, Roonprapunt, and Margolis, 1997).

The class of ‘exceptional mosaics’ is so small in number that it seems possible its existence could be explained through a technical complication of the mosaic analysis. For example, a large nucleolus is characteristic of the excretory cell even in wild type animals, and although Manser and colleagues reported that they could reliably distinguish between excretory cells carrying the duplication and those not carrying it based on nucleolar size (Manser, Roonprapunt, and Margolis, 1997), it remains possible that the five aforementioned mosaics were misclassified with respect to the genotype of the excretory cell. Even if the rescuing chromosomal duplication was not inherited by the excretory cell in each of these animals, a closely related ancestral cell that carried the duplication and expressed MIG-10 could have passed on a sufficient amount of the protein to the excretory cell to fulfill a cell autonomous function vital to canal development. Meiotic recombination between the rescuing chromosomal duplication and native chromosome

III could have caused the wild type copy of *mig-10* to segregate away from the *ncl-1* marker. Some of the gametes produced from such a meiotic event could have given rise to animals that would not have displayed the Mig-10 phenotype due to stable inheritance of wild type *mig-10* and that could still have been mosaics with respect to the remainder of the chromosomal duplication containing the *ncl-1* marker. An absence of the remainder of the chromosomal duplication in the excretory cell of these animals would manifest as a cell with an enlarged nucleolus, and would therefore not have been distinguished from a cell in which the intact chromosomal duplication was absent. These alternative explanations for the existence of the class of ‘exceptional mosaics’ demonstrate that the mosaic analysis could have arrived at an erroneous conclusion regarding the necessity of MIG-10 expression within the excretory cell with respect to canal development.

Further investigation may also reveal that the conclusion from the mosaic analysis suggesting autonomous expression of MIG-10 within the excretory cell is insufficient for rescue of canal outgrowth is not in direct opposition to the conclusion drawn from the experimental results described in this work. The apparent contradiction in these results could be due to differences in the experimental approaches. An advantage to the approach taken by Manser and colleagues is that the rescuing chromosomal duplication employed the endogenous promoter of *mig-10* to direct expression, as opposed to the recombinant vectors used in this analysis that relied on the *pgp-12* promoter to express MIG-10. Expression of MIG-10 by the endogenous promoter essentially guaranteed that the pattern and level of expression of this protein in a wild type animal was recapitulated in an animal carrying the duplication, except in any cells in which the duplication was lost. Thus, even though the results presented in this work show that MIG-10 can function autonomously in the excretory cell to promote canal outgrowth, the protein may not be

expressed endogenously in this cell and may instead rescue canal outgrowth through a different, cell nonautonomous mechanism. Another possibility is that MIG-10 may be expressed endogenously in the excretory cell in an amount much lower than that generated from expression by the *pgp-12* promoter such that full rescue with endogenous expression is only achieved when surrounding cells also express MIG-10.

Such models assume that aside from its characterized role in localizing UNC-34, MIG-10 performs at least one additional function critical for canal outgrowth that is required nonautonomously with respect to the excretory cell. Investigations of other model systems describing the involvement of MRL family members in processes other than cell migration and outgrowth, such as cell adhesion (Lafuente *et al.*, 2004) and cell proliferation (Lyulcheva *et al.*, 2008), suggest that the full range of activities performed by MIG-10, the only MRL family member present in *C. elegans*, may not yet be fully realized. MIG-10 could, for example, have an alternate function similar to that of RIAM, which promotes cell adhesion through an Ena/VASP-independent mechanism involving activation of $\beta 1$ and $\beta 2$ integrins (Lafuente *et al.*, 2004). Junction formation mediated by MIG-10 would be expected to require expression of MIG-10 by the cells surrounding the excretory cell if this process were critical to canal outgrowth. However, the finding that MIG-10 and Lpd do not bind to Rap1 (Quinn, Pfeil, and Wadsworth, 2008), the GTPase recruited by RIAM to promote formation of cell-cell adhesions (Lafuente *et al.*, 2004), suggests that MIG-10 does not function homologously to RIAM.

Additional cell nonautonomous roles in excretory canal development for MIG-10A and/or MIG-10B could have been masked in these experiments as a result of restricting expression to the excretory cell. Experiments similar to those presented in this work could be conducted in which expression of each of these isoforms is expanded to include cells neighboring the excretory cell

to determine if this leads to more complete rescue of posterior canal truncation than was observed in this work. The data presented in Figure 11 indicate that expanding MIG-10 expression outside the excretory cell may indeed allow for more complete rescue. The variability in extent of rescue observed in animals carrying *pgp-12::MIG-10A::GFP*, *pgp-12::MIG-10B::GFP*, or *pgp-12::MIG-10AB::GFP* arrays was much greater than that observed in wild type animals or those carrying FosAB. Since MIG-10A and MIG-10B expression are driven by the endogenous MIG-10 promoter in FosAB animals, expression is not confined to the excretory cell. Thus, the differences in expression pattern between FosAB animals and animals carrying MIG-10A, MIG-10B, and MIG-10AB arrays could explain the observed differences in the variability in the extent of rescue of posterior canal truncation.

Recent evidence suggests that MIG-10B and MIG-10A can rescue different defects of neuronal development, suggesting they may have distinct roles (D. Colón-Ramos, personal communication). The results presented in this work demonstrate that MIG-10A and MIG-10B rescue anterior and posterior excretory canal length to the same extent when expressed autonomously with respect to the excretory cell (Fig. 11). This result suggests that, at least with respect to excretory canal development, these isoforms function redundantly.

The nearly complete rescue of the posterior excretory canals and the complete rescue of the anterior canals achieved by expression of MIG-10A and/or MIG-10B within the excretory cell alone suggest that MIG-10C is not required for excretory canal development, which is in agreement with prior observations (Zhang, 2010). Although the results of the rescue experiments do not rule out the possibility that MIG-10A or MIG-10B may be required cell nonautonomously with respect to the excretory cell to promote canal outgrowth, they strongly suggest that both of these isoforms function cell autonomously. The results therefore provide evidence that MIG-10A

and MIG-10B are likely to be expressed in the excretory cell *in vivo*, a site of expression that has also been suggested for ABI-1 (Schmidt *et al.*, 2009).

The ABI-1 SH3 domain may bind multiple sites in MIG-10 to recruit Abl tyrosine kinase

Just as the results of rescue experiments show that MIG-10A and MIG-10B act redundantly within the excretory cell to promote canal outgrowth, the results of the co-immunoprecipitation analysis demonstrate that both of these isoforms can interact with ABI-1 (Figs. 13, 16, 17).

Furthermore, this analysis revealed that the N-terminus and C-terminal SH3 domain of ABI-1 are the regions in this protein most likely to be necessary for the interaction with MIG-10A.

Preliminary results examining the ability of each of these domains to interact with MIG-10A suggest that the ABI-1 SH3 domain can interact with full length MIG-10A, the MIG-10 variant containing the RA and PH domains, and the C-terminal MIG-10 variant while the ABI-1 N-terminus did not interact with any of these variants. A similar analysis of MIG-10 variants revealed that the RAPH variant and the C-terminal variant both interact with full length ABI-1.

Both the RAPH and C-terminal variants are common to all isoforms of MIG-10, suggesting that the interaction observed between full length MIG-10B and ABI-1 is likely to involve these same regions in MIG-10B (for a summary of results from the co-immunoprecipitation analysis, see Figure 18). Taken together, these results suggest that the SH3 domain of ABI-1 interacts with MIG-10A and MIG-10B through sites within the C-terminus and the region containing the RA and PH domains of MIG-10 (Fig. 19).

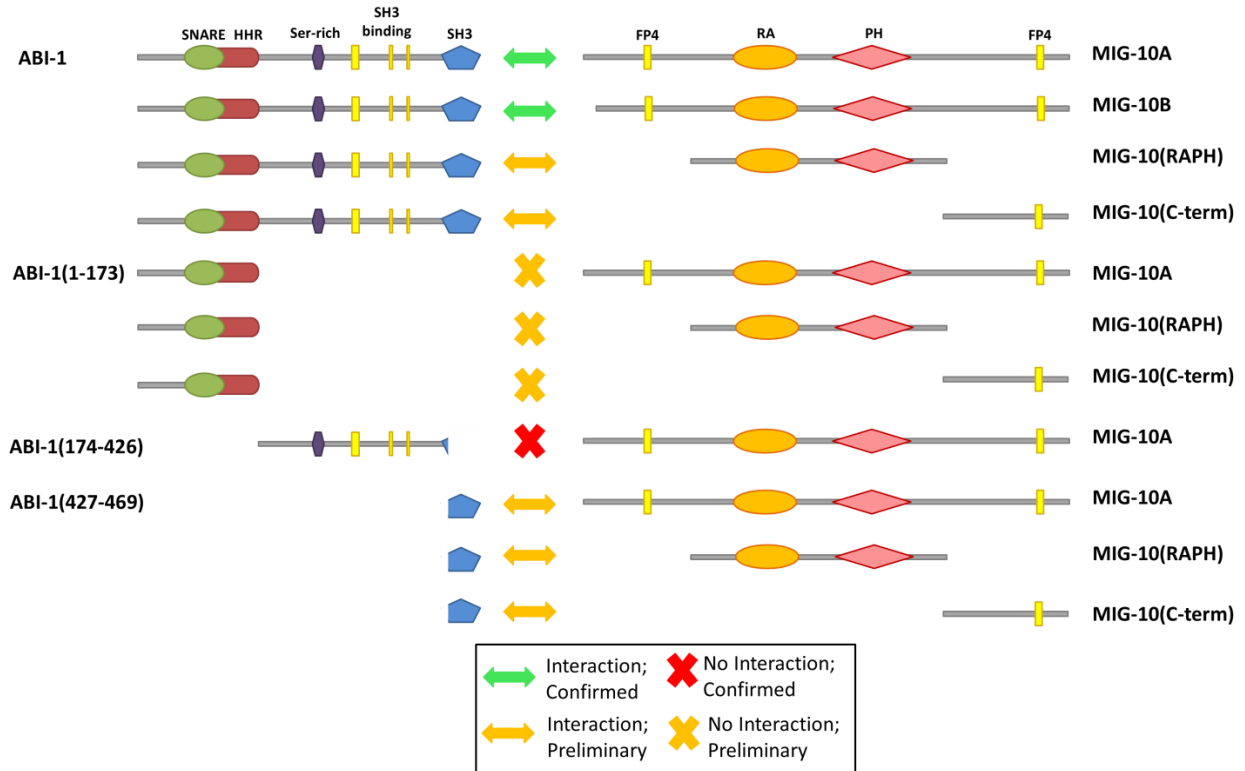


Figure 18: Summary of results from co-immunoprecipitation analysis. The result of each of the combinations of ABI-1 and MIG-10 variants tested is indicated by the symbol between each pair of constructs. Results were considered confirmed if they were observed on more than one repetition of the experiment. Preliminary results were those that were not duplicated.

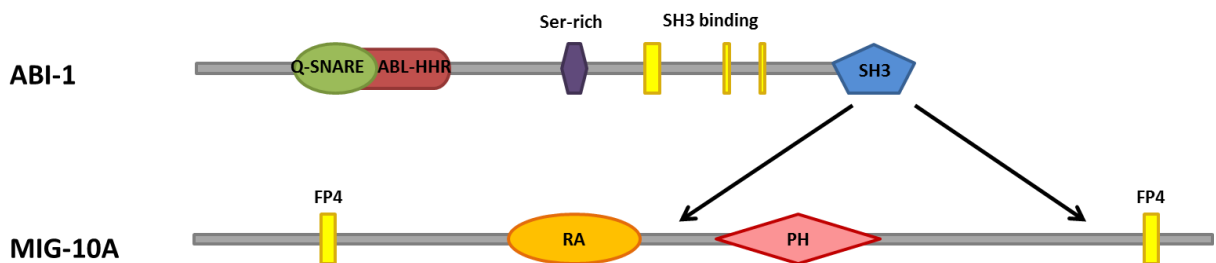


Figure 19: Model of the physical interaction between MIG-10 and ABI-1. Based on the results of co-immunoprecipitation analysis, the SH3 domain of ABI-1 interacts with MIG-10 through both the C-terminus of MIG-10 and the central region containing the RA and PH domains. Although MIG-10A is shown in the schematic, this model of interaction is the same for MIG-10B and MIG-10C because the regions in MIG-10 necessary for the interaction are common to all three isoforms. Proline-rich regions that contain motifs similar to the SH3 binding site consensus PXXP are found in the MIG-10 C-terminus, the central region containing RA and PH domains, and in the N-termini of all three MIG-10 isoforms.

Various ABI-1 variants were previously tested for their ability to interact with MIG-10A in a yeast two hybrid system. The results from this analysis suggested that both the N-terminus and SH3 domain of ABI-1 were necessary for robust interaction with MIG-10A (Table 4; K. Schmidt, personal communication). These results differ from those obtained through co-immunoprecipitation analysis, which suggest the ABI-1 N-terminus is not required for interaction with MIG-10A. It is likely that this discrepancy is due to a false negative result from the co-immunoprecipitation system since the experiment examining the ability of ABI-1(1-173)::GFP to interact with MIG-10A::V5 did not include a positive control. In addition to the N-terminal ABI-1 variant tested in the yeast two-hybrid system that spanned residues 16-173, a longer variant of ABI-1 spanning residues 16-427 was also tested. This longer variant interacted weakly with MIG-10A, suggesting that the ABI-1 N-terminus may actually not be required for interaction with MIG-10A as the results from co-immunoprecipitation analysis suggest. One complication with the interpretation of these results is that protein expression of each variant tested in the yeast two-hybrid system was not verified, meaning the apparent inability of the ABI-1(16-173) variant to interact with MIG-10A in this assay may be due entirely to a lack of expression due to instability of either the ABI-1(16-173) transcript or protein. Both the yeast two-hybrid system and the co-immunoprecipitation system required fusion of variants of interest to either tags or fragments of GAL4, so it is also possible that differences in results from these approaches could be caused by misfolding of the variant of interest in one or both systems.

Table 4: Comparison of yeast two-hybrid and co-immunoprecipitation results examining abilities of ABI-1 variants to interact with MIG-10A. Each row shows ABI-1 variants from the two systems that are most comparable in terms of the region of ABI-1 spanned. “N/A” indicates that no equivalent existed for the variant shown in the same row in the other system.

Y2H Variant (residues)	Interaction with MIG-10A in Y2H System	co-IP Variant (residues)	Interaction with MIG-10A in co-IP system
16-469	Interacts	1-469	Interacts
16-173	Interacts	1-173	Does not interact
174-427	Does not interact	174-426	Does not interact
N/A	N/A	427-469	Interacts
16-427	Interacts weakly	N/A	N/A

The results of co-immunoprecipitation analysis also revealed a potential biochemical consequence of the MIG-10/ABI-1 interaction. An apparent modification to MIG-10A::V5 was consistently observed when this protein was co-expressed with ABI-1::GFP, but not when it was co-expressed with ABI-1(174-426)::GFP (Fig. 13). Phosphorylation is a likely candidate for this modification given the recent evidence that Lamellipodin is phosphorylated by Abl kinase (Michael *et al.*, 2010), the activity of which can be modulated by Abi-1 (Shi, Ålin, and Goff, 1995). For example, vertebrate Abi-1 is known to target the Ena/VASP family member Mena for phosphorylation by Abl (Tani *et al.*, 2003). This evidence, along with the results from co-immunoprecipitation analysis presented in this work, suggest that ABI-1 may serve to link the MIG-10 pathway to regulation by Abl kinase (Fig. 20). The potential effect of Abl activity on this pathway is controversial. Evidence from genetic analyses suggests Abl opposes Ena/VASP activity during cell migration and outgrowth (Bashaw, *et al.*, 2000; Sheffield *et al.*, 2007) while Abl-mediated phosphorylation of Lpd has been suggested to enhance binding to Ena/VASP members, thereby enhancing Ena/VASP activity (Michael *et al.*, 2010).

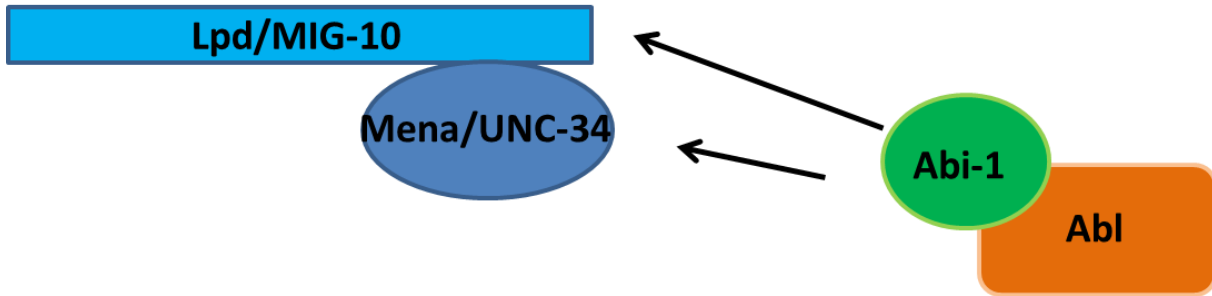


Figure 20: The interaction of ABI-1 with MIG-10 may allow for recruitment of ABL to facilitate phosphorylation of MIG-10. ABI-1 may interact with MIG-10 to promote phosphorylation of MIG-10 by ABL tyrosine kinase. This modification could in turn alter the affinity of MIG-10 for UNC-34, modulating UNC-34 recruitment to the leading edge [in vertebrates, phosphorylation of Lpd increases its affinity for the Ena/VASP family member Mena (Michael *et al.*, 2010)]. Based on data from a vertebrate system, ABI-1 is also likely to bind to UNC-34 to promote its phosphorylation by ABL kinase.

If future experiments reveal that the modification of MIG-10A::V5 is determined to be non-specific, or if it is not the result of phosphorylation, a model for the consequences of the MIG-10/ABI-1 interaction other than that shown in Figure 20 should be considered. ABI-1 is known to interact with many other components of the actin regulatory machinery, such as the Rac-GEF Sos-1 (Scita *et al.*, 1999; Innocenti *et al.*, 2003) and members of the WAVE regulatory complex (Eden *et al.*, 2002; Stovold, Millard, and Machesky, 2005). The interaction of MIG-10 with ABI-1 may therefore serve as a means of connecting one of these other pathways of ABI-1 with that of MIG-10. It is also possible that more than one of these ABI-1 pathways is relevant to the MIG-10/ABI-1 interaction. However, the observation that *mig-10(ct41)* animals treated with *abi-1(RNAi)* have defects in excretory canal outgrowth that are more severe than those observed in *mig-10(ct41)* animals (Grant and Dubuke, 2009) suggests that MIG-10 and ABI-1 are likely to have some functions that are non-overlapping.

It should be noted that the experiments examining the interaction capabilities of ABI-1(1-173)::GFP, ABI-1(427-469)::GFP, MIG-10(RAPH)::V5, and MIG-10(C-term)::V5 must be

repeated in order to confirm the observations reported in this work. A sample of S3 cells co-expressing MIG-10A::V5 and ABI-1::GFP was included as a positive control in the experiment examining the ability of ABI-1(1-173)::GFP to interact with MIG-10A::V5. MIG-10A::V5 did not co-immunoprecipitate with ABI-1::GFP from this sample (Fig. 15), even upon several repetitions of the experiment, suggesting that an error in the experimental system could have prevented MIG-10A::V5 from co-immunoprecipitating with ABI-1(1-173)::GFP. For this reason it is unclear if ABI-1(1-173)::GFP, which encodes the ABI-1 N-terminus fused to GFP, is truly incapable of interacting with MIG-10A. None of the experiments demonstrating that ABI-1(427-469)::GFP, MIG-10(RAPH)::V5, and MIG-10(C-term)::V5 were capable of interaction included a negative control of cells co-expressing ABI-1(174-426)::GFP and MIG-10A::V5 (Figs. 14, 16, 17). Without this control, the possibility that one or more of these results is a false positive cannot be ruled out. In addition, the results from co-immunoprecipitation experiments examining each of these variants were each only observed once, so repetition of these experiments is necessary to confirm the original results.

Technical considerations of co-immunoprecipitation experiments

Attempts to duplicate the aforementioned experiments with the appropriate controls produced inconclusive results in which co-immunoprecipitation was not observed for either the positive control or any samples in which variants were co-expressed with putative interactors. The failure to reproduce these experiments upon multiple attempts highlights the inability of the immunoprecipitation system to yield consistent results. This inconsistency is in turn likely to be the result of inconsistency in one or more of the experimental conditions of the immunoprecipitation system.

Attempts to troubleshoot focused on determining if experimental reagents had deteriorated in such a way as to lead to a complete failure to detect co-immunoprecipitation of MIG-10A::V5 with ABI-1::GFP. Samples were analyzed in duplicate by the same experimental procedure except that one replicate was treated with fresh reagent while the other was treated with pre-existing reagent, and the final results were then compared. This method was applied to assess the quality of the PAS, protease inhibitor cocktail stock, phosphatase inhibitor cocktail stock, buffer stocks, plasmid DNA miniprep stocks used for transfection, or one of the antibody stocks could have led to the sudden failure in signal detection. The results of these optimization experiments indicated there was no difference between pre-existing or fresh reagent for any of these components, suggesting that variability in one of the untested reagents could be the source of inconsistency in the results observed for identical immunoprecipitation experiments. One factor that confounds interpretation of these results is that many of the blots on which bands were not observed in the expected locations displayed uneven signal for a background band across samples, suggesting the blots may have dried out during the detection process, impeding signal production. Precautions should be taken in future experiments to assure that the blots do not dry out during the detection process, such as use of an ample volume of solution for all antibody incubations.

One experimental condition that should be the focus of future optimization is the amount of cells used to prepare each lysate for immunoprecipitation. Each of the samples used in the experiments described in this work consisted of a single well of transfected cells from a 6-well plate. Detection of co-immunoprecipitated proteins could only be achieved using very sensitive HRP substrate solutions optimized for detection of low quantities of protein. Use of a greater number of cells to prepare each lysate for immunoprecipitation could therefore result in isolation

of greater quantities of protein that could be detected with greater ease. If the current amount of V5-tagged protein being recovered on the blots through co-immunoprecipitation is at the lower limit of detection with the HRP substrate solution, it is possible that a slight and consistent decrease in transfection efficiency over time could account for the current failure to reproduce the results of previous immunoprecipitation experiments.

Future experiments

Aside from the issue of inconsistent results, there were two major limitations to the domain-deletion approach used in this work to investigate the interaction between MIG-10 and ABI-1. First, there is a possibility that deletion of one or more domains from either protein altered its conformation such that sites required for interaction were made more or less accessible. Second, the accessibility of regions required for interaction could also have been altered through the introduction of either a GFP or V5 tag. To minimize the effects of deletion, final examinations of the physical requirements for interaction should be made in this system using variants of MIG-10 and ABI-1 in which only the domain(s) necessary for interaction have been deleted. For example, if the preliminary results presented in this work are confirmed, the deletion mutant ABI-1(427-469)::GFP, which lacks the SH3 domain, should be tested for its ability to interact with MIG-10A::V5 and MIG-10B::V5. To eliminate the effects of the introduction of tags, deletion mutants could be generated without tags and tested in the immunoprecipitation system using antibodies that recognize specific epitopes within MIG-10 and ABI-1.

The potential complications associated with domain deletion analysis and the use of tags could be avoided through examination of untagged MIG-10 and ABI-1 variants in which the amino acid sequence has been altered. For each protein, the amino acid sequence within each domain necessary for interaction could be systematically mutated until the minimal sequence necessary

for interaction is identified. Nematodes expressing variants of MIG-10 and ABI-1 in which these sites have been disrupted could then be examined to determine the significance of the interaction *in vivo*. In addition to these experiments, a GST pull down with purified proteins could also be employed to analyze the interaction between MIG-10 and ABI-1. The advantage to use of this system is that evidence of interaction in a pull down implies direct binding of the proteins under examination, whereas the possibility that unidentified proteins are required to mediate the interaction between two proteins observed by co-immunoprecipitation can never be ruled out.

Although a connection between MIG-10 and Abl seems likely based on evidence from the literature, the modification to MIG-10A::V5 reported in this work needs to be investigated more carefully to determine if it is indeed the result of phosphorylation. An experiment has been designed to determine if MIG-10A::V5 is phosphorylated exclusively in the presence of ABI-1::GFP. In this experiment, MIG-10A::V5 immunoprecipitated from cells co-expressing ABI-1::GFP will be treated with calf intestinal phosphatase (CIP) to determine if this increases the electromobility of MIG-10A::V5 to match that of CIP-treated and untreated MIG-10A::V5 immunoprecipitated from cells that did not co-express ABI-1::GFP. Observation of this change would suggest that MIG-10A::V5 is phosphorylated when in the presence of ABI-1::GFP. MIG-10A::V5 immunoprecipitated from cells that co-expressed ABI-1::GFP could then be analyzed by western blotting with an anti-phosphotyrosine antibody to determine if Abl, a tyrosine kinase, could potentially mediate this modification.

The results of this experiment may demonstrate that the observed modification of MIG-10A::V5 is not the result of phosphorylation. In the co-immunoprecipitation system used in this work, the only proteins capable modifying MIG-10A::V5 would have been those expressed endogenously in *D. melanogaster* S3 cells, as MIG-10 and ABI-1 have no known catalytic activities. Although

it seems reasonable that MIG-10 could indeed be a target of *C. elegans* ABL, it seems less likely that the *Drosophila* Abl is capable of interaction with MIG-10. The modification to MIG-10A::V5 observed in S3 cells co-expressing ABI-1::GFP may therefore not involve Abl and/or may have no *in vivo* significance. In the event that the modification is found to be the result of phosphorylation, experiments should be conducted to determine if *C. elegans* ABL is also capable of mediating this modification to be sure that MIG-10 is a specific target of ABL.

Understanding the consequences of the interaction between MIG-10 and ABI-1 will surely serve as a topic for future studies of two proteins that have traditionally been investigated independently of one another. The results presented in this work from rescue analysis and immunoprecipitation experiments suggest that excretory canal development could be one process affected by interaction of these two proteins within the excretory cell (Fig. 21). The observation that MIG-10A::V5 appears to be modified as a result of co-expression with ABI-1::GFP suggests that ABI-1 could serve to connect MIG-10A with components of other regulatory pathways, such as Abl. Further analysis of the intricacies of this interaction will therefore contribute to a better understanding of how the complex processes of cell migration and outgrowth are regulated on a broad scale involving multiple signaling pathways.

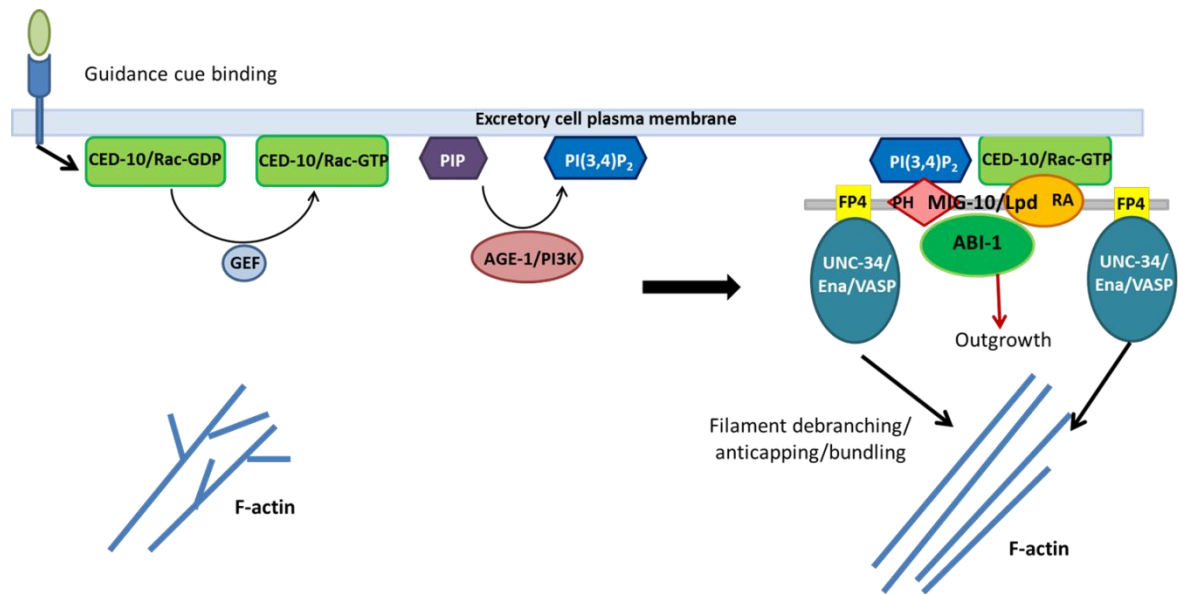


Figure 21: MIG-10 and ABI-1 are likely to function together to promote excretory canal outgrowth through a cell autonomous mechanism.

References

- Adler, C.E., Fetter, R.D., and Bargmann, C.I. (2006). UNC-6/Netrin induces neuronal asymmetry and defines the site of axon formation. *Nat Neurosci* **9**:511-518.
- Altun, Z.F. and Hall, D.H. 2009. Excretory system. In *WormAtlas*.
<http://dx.doi.org/10.3908/wormatlas.1.17>
- Bashaw, G.J., Kidd, T., Murray, D., Pawson, T., and Goodman, C.S. (2000). Repulsive axon guidance: Abelson and Enabled play opposing roles downstream of the Roundabout receptor. *Cell* **101**:703-715.
- Bielas, S., Higginbotham, H., Koizumi, H., Tanaka, T., and Gleeson, J.G. (2004). Cortical neuronal migration mutants suggest separate but intersecting pathways. *Annu Rev Cell Dev Biol* **20**: 593-618.
- Blagg, S.L., Stewart, M., Sambles, C., and Insall, R.H. (2003). PIR121 regulates pseudopod dynamics and SCAR activity in *Dictyostelium*. *Curr Biol* **13**:1480-1487.
- Brenner, S. (1974). The genetics of *Caenorhabditis elegans*. *Genetics* **77**: 71-94.
- Buechner, M. (2002). Tubes and the single *C. elegans* excretory cell. *Trends Cell Biol* **12**: 479-484.
- Chan, S.S.-Y., Zheng, H., Su, M.-W., Wilk, R., Killeen, M.T., Hedgecock, E.M., and Culotti, J.G. (1996). UNC-40, a *C. elegans* homolog of DCC (Deleted in Colorectal Cancer), is required in motile cells responding to UNC-6 Netrin cues. *Cell* **87**: 187-195.
- Chang, C., Adler, C.E., Krause, M., Clark, S.G., Gertler, F.B., Tessier-Lavigne, M., and Bargmann, C.I. (2006). MIG-10/Lamellipodin and AGE-1/PI3K promote axon guidance and outgrowth in response to Slit and Netrin. *Curr Biol* **16**:854-862.
- Chen, Z., Borek, D., Padrick, S.B., Gomez, T.S., Metlagel, Z., Ismail, A.M., Umetani, J., Billadeau, D.D., Otwinowski, Z., and Rosen, M.K. (2010). Structure and control of the actin regulatory WAVE complex. *Nature* **468**:533-538.
- Drees, F. and Gertler, F.B. (2008). Ena/VASP: proteins at the tip of the nervous system. *Curr Opin Neurobiol* **18**:53-59.
- Dubuke, M. and Grant, C. (2009). ABI-1 interacts with MIG-10: protein interaction in neuronal migration in *Caenorhabditis elegans*. Senior Undergraduate MQP. Worcester, MA: Worcester Polytechnic Institute.

- Echarri, A., Lai, M.J., Robinson, M.R., and Pendergast, A.M. (2004). Abl Interactor 1 (Abi-1) Wave-binding and SNARE domains regulate its nucleocytoplasmic shuttling, lamellipodium localization, and Wave-1 levels. *Mol Cell Biol* **24**:4979-4993.
- Eden, S., Rohatgi, R., Podtelejnikov, A.V., Mann, M., Kirschner, M.W. (2002). Mechanism of regulation of WAVE1-induced actin nucleation by Rac1 and Nck. *Nature* **418**:790-793.
- Engle, E.C. (2010). Human genetic disorders of axon guidance. *Cold Spring Harb Perspect Biol*. **2**: a001784.
- Fleming, T., Chien, S.-C., Vanderzalm, P.J., Dell, M., Gavin, M.K., Forrester, W.C., and Garriga, G. (2010). The role of *C. elegans* Ena/VASP homolog UNC-34 in neuronal polarity and motility. *Dev Biol* **344**:94-106.
- Goley, E.D. and Welch, M.D. (2006). The ARP2/3 complex: an actin nucleator comes of age. *Nat Rev Mol Cell Biol* **7**:713-726.
- Gosselin, J. and O'Toole, S. (2008). MIG-10, an adaptor protein, interacts with ABI-1, a component of actin polymerization machinery. Senior Undergraduate MQP. Worcester, MA: Worcester Polytechnic Institute.
- Hao, J.C., Yu, T.W., Fujisawa, K., Culotti, J.G., Gengyo-Ando, K., Mitani, S., Moulder, G., Barstead, R., Tessier-Lavigne, M., and Bargmann, C.I. (2001). *C. elegans* Slit acts in midline, dorsal-ventral, and anterior-posterior guidance via the SAX-3/Robo receptor. *Neuron* **32**:25-38.
- Hashmi, S. and Kuhlwein, M. (2011). MIG-10 and UNC-53: two proteins involved in the migration of neurons and the excretory canal. Senior Undergraduate MQP. Worcester, MA: Worcester Polytechnic Institute.
- Hedgecock, E.M., Culotti, J.G., and Hall, D.H. (1990). The *unc-5*, *unc-6*, and *unc-40* genes guide circumferential migrations of pioneer axons and mesodermal cells on the epidermis in *C. elegans*. *Neuron* **4**: 61-85.
- Hedgecock, E.M., Culotti, J.G., Hall, D.H., and Stern, B.D. (1987). Genetics of cell and axon migrations in *Caenorhabditis elegans*. *Development* **100**: 365-382.
- Innocenti, M., Frittoli, E., Ponzanelli, I., Falck, J.R., Brachmann, S.M., Di Fiore, P.P., and Scita, G. (2003). Phosphoinositide 3-kinase activates Rac by entering in a complex with Eps8, Abi1, and Sos-1. *J Cell Biol* **160**:17-23.
- Innocenti, M., Zucconi, A., Disanza, A., Frittoli, E., Areces, L.B., Steffen, A., Stradal, T.E.B., Di Fiore, P.P., Carrier, M.-F., and Scita, G. (2004). Abi1 is essential for the formation and activation of a WAVE2 signalling complex. *Nat Cell Biol* **6**:319-327.

- Ismail, A.M., Padrick, S.B., Chen, B., Umetani, J., and Rosen, M.K. (2009). The WAVE regulatory complex is inhibited. *Nat Struct Mol Biol* **16**:561-563.
- Kolodkin, A.L. and Tessier-Lavigne, M., ed. (2010). Mechanisms and molecules of neuronal wiring: a primer. *Cold Spring Harb Perspect Biol* doi: 10.1101/cshperspect.a001727.
- Krause, M., Leslie, J.D., Stewart, M., Lafuente, E.M., Valderrama, F., Jagannathan, R., Strasser, G.A., Rubinson, D.A., Liu, H., Way, M., Yaffe, M.B., Boussiotis, V.A., and Gertler, F.B. (2004). Lamellipodin, an Ena/VASP ligand, is implicated in the regulation of lamellipodial dynamics. *Dev Cell* **7**:571-583.
- Lafuente, E.M., van Puijenbroek, A.A., Krause, M., Carman, C.V., Freeman, G.J., Berezovskaya, A., Constantine, E., Springer, T.A., Gertler, F.B., and Boussiotis, V.A. (2004). RIAM, an Ena/VASP and Profilin ligand, interacts with Rap1-GTP and mediates Rap1-induced adhesion. *Dev Cell* **7**:585-595.
- Leng, Y., Zhang, J., Badour, K., Arpaia, E., Freeman, S., Cheung, P., Siu, M., and Siminovitch, K. (2005). Abelson-interactor-1 promotes WAVE2 membrane translocation and Abelson-mediated tyrosine phosphorylation required for WAVE2 activation. *Proc Natl Acad Sci* **102**:1098-1103.
- Levy-Strumpf, N., and Culotti, J.G. (2007). VAB-8, UNC-73 and MIG-2 regulate axon polarity and cell migration functions of UNC-40 in *C. elegans*. *Nat Neurosci* **10**:161-168.
- Lin, T.-Y., Huang, C.-H., Kao, H.-H., Liou, G.-G., Yeh, S.-R., Cheng, C.-M., Chen, M.-H., Pan, R.-L., and Juang, J.-L. (2009). Abi plays an opposing role to Abl in *Drosophila* axonogenesis and synaptogenesis. *Development* **136**:3099-3107.
- Lylulcheva, E., Taylor, E., Michael, M., Vehlow, A., Tan, S., Fletcher, A., Krause, M., and Bennett, D. (2008). *Drosophila* Pico and its mammalian ortholog Lamellipodin activate serum response factor and promote cell proliferation. *Dev Cell* **15**:680-690.
- MacNeil, L.T., Hardy, R.W., Pawson, T., Wrana, J.L., and Culotti, J.G. (2009). UNC-129 regulates the balance between UNC-40 dependent and independent UNC-5 signaling pathways. *Nat Neurosci* **12**:150-155.
- Manser, J. and Wood, W.B. (1990). Mutations affecting embryonic cell migrations in *Caenorhabditis elegans*. *Dev Gen* **11**: 49-64.
- Manser, J., Roonprapunt, C., and Margolis, B. (1997). *C. elegans* cell migration gene *mig-10* shares similarities with a family of SH2 domain proteins and acts cell nonautonomously in excretory canal development. *Dev Biol* **184**: 150-164.

- Michael, M., Vehlow, A., Navarro, C., and Krause, M. (2010). c-Abl, Lamellipodin, and Ena/VASP proteins cooperate in dorsal ruffling of fibroblasts and axonal morphogenesis. *Curr Biol* **20**:783-791.
- Nelson, F.K. and Riddle, D.L. (1984). Functional study of the *Caenorhabditis elegans* secretory-excretory system using laser microsurgery. *J Exp Zool* **231**: 45-56.
- Oikawa, T., Yamaguchi, H., Itoh, T., Kato, M., Ijuin, T., Yamazaki, D., Suetsugu, S., and Takenawa, T. (2004). PtdIns(3,4,5)P₃ binding is necessary for WAVE2-induced formation of lamellipodia. *Nat Cell Biol* **6**:420-426.
- Ou, G. and Vale, R.D. (2009). Molecular signatures of cell migration in *C. elegans* Q neuroblasts. *J Cell Biol* **185**:77-85.
- Pan, C.-L., Howell, J.E., Clark, S.G., Hilliard, M., Cordes, S., Bargmann, C.I., and Garriga, G. (2006). Multiple Wnts and Frizzled receptors regulate anteriorly directed cell and growth cone migrations in *Caenorhabditis elegans*. *Dev Cell* **10**: 367-377.
- Purves, D., Augustine, G.J., Fitzpatrick, D., Katz, L.C., LaMantia, A.-S., McNamara, J.O., and Williams, S.M., eds. (2001). *Neuroscience*, 2nd Edition. Sunderland, MA: Sinauer Associates, Inc.
- Quinn, C.C., Pfeil, D.S., and Wadsworth, W.G. (2008). CED-10/Rac1 mediates axon guidance by regulating the asymmetric distribution of MIG-10/Lamellipodin. *Curr Biol* **18**:808-813.
- Quinn, C.C., Pfeil, D.S., Chen, E., Stovall, E.L., Harden, M.V., Gavin, M.K., Forrester, W.C., Ryder, E.F., Soto, M.C., and Wadsworth, W.G. (2006). UNC-6/Netrin and SLT-1/Slit guidance cues orient axon outgrowth mediated by MIG-10/RIAM/Lamellipodin. *Curr Biol* **16**:845-853.
- Quinn, Q.C., and Wadsworth, W.G. (2008). Axon guidance: asymmetric signaling orients polarized outgrowth. *Trends Cell Biol* **18**:597-603.
- Rogers, S.L, Wiedemann, U., Stuurman, N., and Vale, R.D. (2003). Molecular requirements for actin-based lamella formation in *Drosophila* S2 cells. *J Cell Biol* **162**:1079-1088.
- Ryu, J.R., Echarri, A., Li, R., and Pendergast, A.M. (2009). Regulation of cell-cell adhesion by Abi/Diaphanous complexes. *Mol Cell Biol* **29**:1735-1748.
- Sanes, D.H., Reh, T.A., and Harris, W.A. (2006). *Development of the Nervous System*, 2nd Edition. London: Elsevier Academic Press.
- Schmidt, K.L., Marcus-Gueret, N., Adeleye, A., Webber, J., Baillie, D., and Stringham, E.G. (2009). The cell migration molecule UNC-53/NAV2 is linked to the ARP2/3 complex by ABI-1. *Development* **136**:563-574.

- Scita, G., Nordstrom, J., Carbone, R., Tenca, P., Giardina, G., Gutkind, S., Bjarnegard, M., Betsholtz, C., and Di Fiore, P.P. (1999). EPS8 and E3B1 transduce signals from Ras to Rac. *Nature* **401**:290-293.
- Sheffield, M., Loveless, T., Hardin, J., and Pettitt, J. (2007). *C. elegans* Enabled exhibits novel interactions with N-WASP, Abl, and cell-cell junctions. *Curr Biol* **17**:1791-1796.
- Shi, Y., Ålin, K., and Goff, S.P. (1995). Abl-interactor-1, a novel SH3 protein binding to the carboxy-terminal portion of the Abl protein, suppresses v-abl transforming activity. *Genes Dev* **9**:2583-2597.
- Steffen, A., Rottner, K., Ehinger, J., Innocenti, M., Scita, G., Wehland, J., and Stradal, T.E.B. (2004). Sra-1 and Nap1 link Rac to actin assembly driving lamellipodia formation. *EMBO* **23**:749-759.
- Stovold, C.F., Millard, T.H., and Machesky, L.M. (2005). Inclusion of Scar/WAVE3 in a similar complex to Scar/WAVE1 and 2. *BMC Cell Biol* **6**:11.
- Sullivan-Keizer, J. (2009). Analysis of *mig-10* interactors. Senior Undergraduate MQP. Worcester, MA: Worcester Polytechnic Institute.
- Takenawa, T. and Suetsugu, S. (2007). The WASP-WAVE protein network: connecting the membrane to the cytoskeleton. *Nat Rev Mol Cell Biol* **8**:37-48.
- Tani, K., Sato, S., Sukezane, T., Kojima, H., Hirose, H., Hanafusa, H., and Shishido, T. (2003). Abl Interactor 1 promotes tyrosine 296 phosphorylation of mammalian Enabled (Mena) by c-Abl kinase. *J Biol Chem* **278**:21685-21692.
- Tanos, B.E. and Pendergast, A.M. (2007). Abi-1 forms an epidermal growth factor-inducible complex with Cbl: role in receptor endocytosis. *Cell Signaling* **19**:1602-1609.
- Wadsworth, W.G., Bhatt, H., and Hedgecock, E.M. (1996). Neuroglia and pioneer neurons express UNC-6 to provide global and local netrin cues for guiding migrations in *C. elegans*. *Neuron* **16**:35-46.
- Watari-Goshima, N., Ogura, K., Wolf, F.W., Goshima, Y., and Garriga, G. (2007). *C. elegans* VAB-8 and UNC-73 regulate the SAX-3 receptor to direct cell and growth-cone migrations. *Nat Neurosci* **10**:169-176.
- Whangbo, J. and Kenyon, C. (1999). A Wnt signaling system that specifies two patterns of cell migration in *C. elegans*. *Mol Cell* **4**:851-858.
- Wood, W.B., ed. (1988). *The Nematode Caenorhabditis elegans*. New York: Cold Spring Harbor Laboratory.

Zhang, Subaiou. (2010). Functional analysis of MIG-10: a cytoplasmic adaptor protein important in neuronal migration and process outgrowth in *C. elegans*. Senior Undergraduate MQP. Worcester, MA: Worcester Polytechnic Institute.

Zhao, Z., Fang, L., Chen, N., Johnsen, R.C., Stein, L., and Baillie, D.L. (2005). Distinct regulatory elements mediate similar expression patterns in the excretory cell of *Caenorhabditis elegans*. *J Biol Chem* **280**:38787-38794.